Aus der Klinik für Neurologie (Abteilung Experimentelle Neurologie) der
Medizinischen Fakultät Charité – Universitätsmedizin Berlin

DISSERTATION

Effects of human anti-GluN1 antibodies on the offspring in a murine model of maternal antibody transfer

zur Erlangung des akademischen Grades
Doctor of Philosophy (PhD)
im Rahmen des
International Graduate Program Medical Neuroscience

vorgelegt der Medizinischen Fakultät
Charité – Universitätsmedizin Berlin

von

Betty Jurek, geb. Becker

aus Gerolstein

Datum der Promotion: 07.12.2018

„Der Beginn aller Wissenschaft ist das Erstaunen, dass die Dinge sind, wie sie sind.“

Aristoteles

Index of contents/Inhaltsverzeichnis

Figure index

Abstract

Autoantibodies (AB) against the essential GluN1 subunit of the glutamatergic *N*-methyl-D-aspartate receptor (NMDAR) are among commonly diagnosed neuronal AB also in healthy individuals creating a considerable subgroup of pregnant women potentially transferring these AB during pregnancy to their fetus.

In this study, we established a murine model of maternal AB transfer in order to investigate the effects of human GluN1 AB on the development of the offspring. Therefore, 240 µg of patient-derived, monoclonal GluN1 AB or an isotype-matched non-reactive control (CTL) AB was injected into pregnant C57BL/6J dams at gestational days E13 and E17. Physiological, developmental and behavioral parameters in the offspring were investigated for AB-mediated effects at different developmental stages (E19, P0-P14, adulthood and old age).

Indeed, GluN1 AB were enriched in neonatal circulation and brain parenchyma, leading to considerably reduced NMDAR densities (up to 49.2%) in early neonatal life and reducing amplitudes of spontaneous excitatory postsynaptic currents in acute slices. Exposure to GluN1 AB increased mortality (+27%) within the first postnatal days, impaired establishment of neonatal reflexes and reduced bodyweight during neonatal life and adolescence. AB interaction also caused profound changes persisting into adulthood as GluN1 AB-treated offspring displayed significantly decreased brain volumes (total brain, cerebral cortex, cerebellum, and brain stem) and had altered behavioral profiles of hyperactivity, reduced anxiety and impaired pre-pulse inhibition.

This murine model proves the pathogenicity of maternally transferred GluN1 AB by causing developmental deficits in early life with long-lasting changes persisting into late adulthood. It might offer an explanation for various features of unclear developmental abnormalities also in humans and builds the basis for further evaluation of prevalence and relevance of GluN1 AB in pregnant women.

Zusammenfassung

Autoantikörper (AK) gegen die essentielle Untereinheit GluN1 des glutamatergen *N*-Methyl-D-Aspartat-Rezeptors (NMDAR) zählen zu den häufig diagnostizierten anti-neuronalen AK auch in der gesunden Bevölkerung. Damit besteht eine große Wahrscheinlichkeit, dass auch schwangere Frauen diesen AK tragen und ihn während der Schwangerschaft auf ihren Fötus über die Plazenta transferieren.

Um das Potenzial dieser GluN1 AK zu evaluieren, entwickelten wir ein Mausmodell des maternalen GluN1-AK-Transfers. Dabei wurden je 240 µg eines humanen, monoklonalen GluN1-AK oder eines entsprechenden nicht-reaktiven Kontrollantikörpers in trächtige C57BL/6J Mäuse am 13. und 17. Tag der Trächtigkeit injiziert und die Auswirkungen auf die Nachkommen hinsichtlich Physiologie, Entwicklung und Verhalten zu unterschiedlichen Zeitpunkten ihrer Entwicklung (E19, P0-P14, Erwachsenenalter und fortgeschrittenes Alter) untersucht.

Dabei zeigte sich nicht nur, dass der AK in hoher Konzentration übertragen wurde, sondern sogar eine Anreicherung der AK im neonatalen Blutkreislauf und Hirngewebe erfolgte, was zur einer ausgeprägten Reduktion von NMDAR (bis zu 49,2%) führte und die Amplituden von spontanen exzitatorischen postsynaptischen Strömen verringerte. Zudem erhöhten GluN1-AK die Mortalität (+27%), verzögerten die Ausbildung neonataler Reflexe und verringerten das Körpergewicht der murinen Nachkommen bis zum Erwachsenenalter. Die von dem Muttertier übertragenen AK führten nicht nur zu Einschränkungen in der Postnatalphase der Nachkommen, sondern verursachten auch weitreichende Änderungen im Erwachsenenalter, da sie zu einer Reduktion der Hirnvolumina (Gesamthirnvolumen, zerebraler Cortex, Kleinhirn und Hirnstamm) und einem veränderten Verhaltensprofil mit Hyperaktivität, reduziertem Angstverhalten und Störungen des sensomotorischen Gatings führten.

Mit diesem Tiermodell konnte die Pathogenität maternaler GluN1 AK nachgewiesen werden, die nicht nur die frühe Entwicklung der Nachkommen schädigten, sondern auch zu langanhaltenden Veränderungen bis ins Erwachsenenalter führten. Diese Arbeit bietet eine mögliche Erklärung für vielgestaltige entwicklungsbedingte Störungen beim Menschen und bildet die Basis für weitere Untersuchungen, um die Häufigkeit und die Relevanz von AK gegen GluN1 in schwangeren Frauen zu untersuchen.

Abbreviation

AB	Antibody/antibodies
AMPAR	α-amino-3-hydroxy-5-methyl-4-isoxazolepropionic acid receptor(s)
APS	Ammonium persulfate
APV	(2R)-amino-5-phosphonovaleric acid (NMDAR antagonist)
ASD	Autism spectrum disorders
BDNF	Brain-derived neurotrophic factor
BSA	Bovine serum albumin
CA1/CA3	*Cornu Ammon*= Ammon's horn (hippocampal region)
CaMKII	Ca^{2+}/calmodulin-dependent protein kinase II
CASPR2	Contactin-associated protein 2
CD31	Cluster of differentiation 31
CNS	Central nervous system
CREB	Ca^{2+}/calmodulin-dependent protein kinase - cAMP response element binding protein
CSF	Cerebral spinal fluid
CTL	Control
CTX	Cerebral cortex
DAPI	4′,6-diamidino-2-phenylindole
DMEM	Dulbecco's Modified Eagle's medium
ELISA	Enzyme-linked immunosorbent assay
EPSC	Excitatory postsynaptic current
EXF	Extraction fraction
FACS	Fluorescence-activated cell sorting
FBS	Fetal bovine serum
FcRn	Neonatal Fc-receptor
GluN1/NR1	*N*-Methyl-D-Aspartate receptor subunit GluN1
gp	Guinea pig
HEK (cells)	Human embryonic kidney cells
HRP	Horseradish peroxidase
hum	Human
IgG	Immunoglobulin G
IHC	Immunohistochemistry
LD	Learning disabilities
mc	Monoclonal
MK-801	Dizocilpine (NMDAR antagonist)
MRI	Magnetic resonance imaging
ms	Mouse
NDS	Neurodevelopmental Scoring
NGS	Normal goat serum
NMDAR	*N*-Methyl-D-Aspartate receptor(s)
pc	Polyclonal

PCP	Phencyclidine (NMDAR antagonist)
PLL	Poly-L lysine
PSD95	Post-synaptic density protein 95
PXF	Pre-extraction fraction
rb	Rabbit
SDS-PAGE	Sodium dodecyl sulfate polyacrylamide gel electrophoresis
TEMED	Tetramethylethylenediamine
VGLUT1	Vesicular glutamate transporter 1
WB	Western Blot

1. Introduction

1.1 *N*-methyl-D-aspartate receptor (NMDAR)

1.1.1 General properties

NMDAR is one of three subtypes of ionotropic, glutamatergic receptors that are mainly responsible for excitatory transmission within the mammalian central nervous system (CNS). In contrast to the other two glutamate-binding ion channels α-amino-3-hydroxy-5-methyl-4-isoxazolepropionic acid receptor (AMPAR) and kainate receptor, NMDAR needs co-activation of both glutamate and glycine (or D-serine) for opening of the ion channel (ligand-binding activation, see Figure 1) [1]. Additionally, NMDAR activation is also voltage-dependent as Mg^{2+} blocks the channel and is only released upon membrane depolarization [2] mediated by mainly AMPAR. Channel opening leads to a voltage-dependent flow of Ca^{2+}, Na^{+}, and K^{+}-ions, with the influx of Ca^{2+} ions being of particular importance as they trigger intracellular signaling pathways [3]. This initiation of signal transduction cascades by NMDAR modulates synaptic strength and plasticity, making NMDAR crucial for processes involved in learning and memory [4].

1.1.2 Structure and subunit arrangement of NMDAR

Classical NMDAR are di-heteromeric ion channels, consisting of two obligatory glycine-binding GluN1 subunits and two glutamate-binding GluN2 subunits (A-D) and are widely expressed throughout the CNS. However, tri-heteromeric combinations (GluN1/GluN2A/GluN2B) are also commonly expressed in the adult brain especially in hippocampus and cortex [5]. Combination with GluN3 (A/B) are less common: tri-heteromeric GluN1/GluN2/GluN3 receptors display profound decreased Ca^{2+}-influx and reduced sensitivity to Mg^{2+} block and are mainly found in astrocytes and oligodendrocytes, enabling glia cells to be activated at physiological resting potentials [6]. Di-heteromeric GluN1/GluN3 glycine-receptors show only very low Ca^{2+} influx and are resistant to blockage by Mg^{2+} *in vitro* and their role in the mammalian CNS is still unclear [7].

In general, NMDAR composition is dependent on developmental status and cell localization accompanied with different channel properties. Di-heteromeric NMDAR with GluN2A or GluN2B show higher conductance openings with higher Mg^{2+} blocking sensitivity and Ca^{2+} permeability as GluN2C or GluN2D containing receptors [7]. Also deactivation kinetics are composition-dependent as excitatory postsynaptic current

(EPSC) decay ranges from 40 ms for GluN1/GluN2A, over 300 ms for GluN1/2B and GluN1/2C to 2s for GluN1/GluN2D receptors [7]. GluN2A and GluN2B are mainly expressed in the adult CNS especially in higher brain regions like cortex and hippocampus, making these subunits critical for proper function of synaptic plasticity [8]. In rodents and humans, GluN1/GluN2B receptors with longer opening times are predominantly expressed during prenatal life with GluN1/GluN2A being almost absent. After birth, increase of GluN1/GluN2A expression paralleled with a potential decrease GluN1/GluN2B, leads to a "GluN2B/GluN2A- switch" that enables fast learning in the immediate postnatal period when neuronal plasticity is of decisive importance [9].

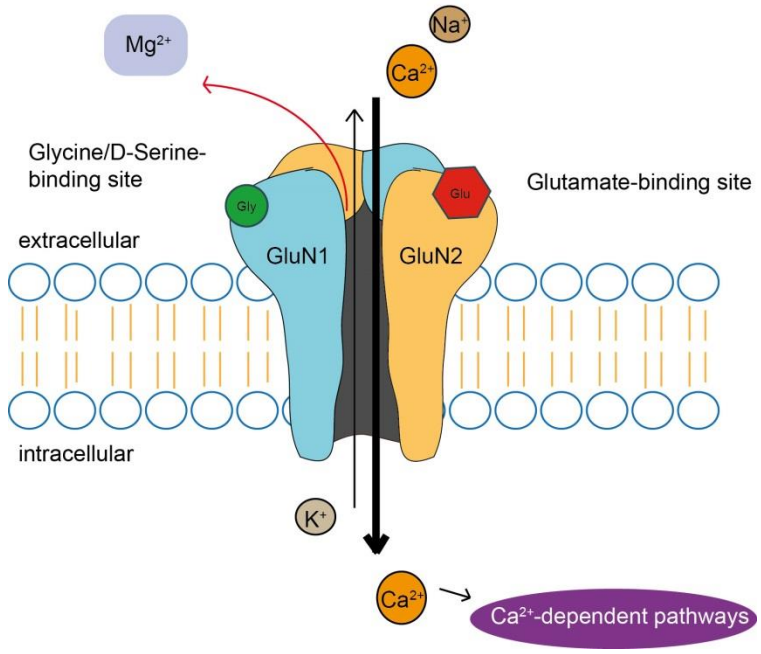

Figure 1: Schematic drawing of NMDAR.
A classical NMDAR consist of 2 GluN1- and 2 GluN2- (A-D) subunits. Upon co-activation by glutamate (red hexagon) and glycine or D-serine (green circle), additional depolarization is needed, to repel channel-blocking Mg^{2+} and allow ionic flow. Thereby, efflux of K^+ and influx of Na^+ and Ca^{2+} is facilitated. Ca^{2+}-flux is of special importance as it triggers different signaling cascades related to e.g. neuronal plasticity and neuronal survival.

1.1.3 GluN1 subunit

GluN1 subunits occur in eight isoforms due to different splicing variants (GluN1-1a/b – GluN1-4a/b) from gene locus GRIN1 on chromosome 9 in humans, with GluN1-1a being the most abundant form [7]. Similar to the other subunits, GluN1 consists of the amino terminal domain (ATD) involved in channel assembly and modulation, the ligand-binding domain (LBD), a transmembrane domain (TMD) and a C-terminal domain (CTD) associated with receptor trafficking and signaling (see Figure 2).

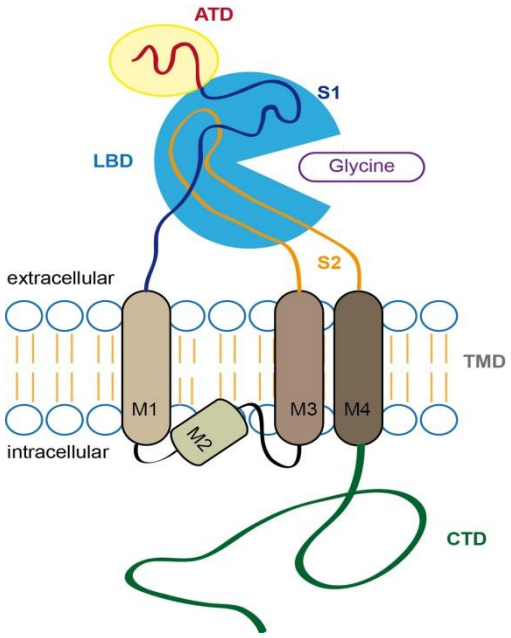

Figure 2: Membrane topology of GluN1 subunit.
On the extracellular surface, N (amino)-terminal domain (ATD, red) and ligand binding domain (LBD, turquoise), consisting of S1 (orange) and S2 (blue), are located. S1 and S2 are anchored to transmembrane domain (TMD, grey), consisting of 3 α helical segments (M1, M3, M4) and a M2 loop. On intracellular site, C-terminal domain (CTD, green) is anchored to M4.

1.2 Temporal expression of NMDAR

GluN1 subunits are essential for NMDAR formation resulting in an ubiquitous expression in the brain. In rodents, studies form in- situ hybridization in rat brain revealed GluN1 expression starting from gestational day E14, peaking at postnatal week 3 with marginal reduced levels through adulthood [10, 11].

Information about expression in humans is less detailed due to limited access to brain tissue. Jantzie and colleagues examined expression of several subunits by western blot analysis of postmortem human brains from postconceptional week (PCW) 20 through adulthood and revealed highest concentration of GluN1 in preterm period (PWC 20-45) compared to adulthood in white matter (+567%) [12]. In grey matter there was no significant difference between distinct developmental stages but a general considerable increase (+1259%) compared to adulthood. This is clearly different from rodent situation as levels of GluN1 remain high also during adulthood.

1.3 NMDAR function

Physiologically, NMDAR are expressed within the entire CNS with hippocampus, cortex, cerebellum, and brain stem representing brain regions of highest receptor density [11]. The unique features of NMDAR namely co-ligand-activation, voltage-dependency and considerable Ca^{2+} influx modulating signaling pathways in the postsynaptic cell making NMDAR (both ionotropic and metabotropic) to the key players for synaptic plasticity. Strengthening neuronal connections by NMDAR is facilitated by

a mechanism called long-term potentiation (LTP) which was first discovered in hippocampal neurons in rabbits [13]. Lømo and Bliss stimulated presynaptic fibers in the prefrontal cortex and made the unexpected observation that the postsynaptic cells in the dentate gyrus showed a long-lasting increased EPSC, if a train of high-frequency stimuli was applied to the presynaptic fibers [13]. Excessive studies especially in hippocampal neurons of CA1 and CA3 region revealed the underlying mechanisms that take place at the synaptic cleft: First, glutamate is released from the pre-synaptic neuron and binds to glutamatergic receptors on the postsynaptic neuron. Second, at this stage it mainly activates fast AMPAR leading to channel opening and flow of ions, where especially influx of Na^+ contributes to cell membrane depolarization. Third, if AMPAR are activated in short intervals, Mg^{2+} that blocks the pore gets repelled leading to channel opening ion transport most importantly Ca^{2+} influx. Fourth, infiltrated calcium initiates cascades of internal signaling leading to long-term changes in the postsynaptic neuron, e.g. insertion of more AMPAR in the postsynaptic density (PSD), increasing the EPCS and strengthening the synapse.

The opposite mechanism is called long-term depression (LTD) and in conjunction with LTP modulates synaptic plasticity [14].

1.4 NMDAR malfunction in disease context

1.4.1 Anti-NMDAR encephalitis (NMDARE)

NMDARE is a condition caused by autoantibodies in the CSF directed against the GluN1 subunit of the NMDAR. Patients experience a typical clinical course starting with infection-like symptoms, e.g. headaches, fever rapid accompanied by psychiatric symptoms like hallucinations. As the disease progresses, patients show severe neurological deficits, e.g. dyskenisia, epileptic seizures and loss of autonomic functions, hypoventilation, loss of consciousness etc., often leading to intensive care treatment [15]. NMDARE was first described by Josep Dalmau and colleagues in 2007 associating immunoglobulin G (IgG) GluN1 AB causal for encephalitis in female patients with ovarian teratoma [15]. Indeed, epidemiologically, NMDARE is most common in young females (81%) with a tumor association of 38% and mean age of onset 21 years determined by a study investigating 577 cases from 2007-2012 [16]. Previous studies have shown that AB from NMDARE patients bind to ATD and a point

mutation of amino acid 368 from asparagine (N) to glutamine (Q) diminishes binding (Figure 2), indicating that this mutation leads to conformational changes, hindering AB binding [17]. As NMDARE is mediated by autoantibodies, first-line therapy is based on application of steroids, intravenous immunoglobulin and performing plasmapheresis. If first-line treatment is unsuccessful, second-line immunotherapy therapeutics from cancer treatment (rituximab, cyclophosphamide) are used. But a standard therapy or even curative therapeutics are missing and due to the absence of an adequate animal model, potential therapeutics have not been tested in animals so far.

In vitro studies revealed the underlying mechanism of NMDARE: AB-mediated NMDAR internalization leads to acute NMDAR hypofunction causing severe neurological deficits and autonomic dysfunction [18, 19]. Application of patients' CSF into the ventricles of mice resulted also in NMDAR reduction *in vivo*, leading to memory deficits and anhedonic depression-like behavior [20]. Kreye and colleagues finally proved that GluN1 AB are sufficient for NMDARE pathogenesis, by isolation of AB-producing cells from patients' CSF, recombinant expression of the distinct monoclonal AB and functional characterization [21]. This AB-repertoire analysis also revealed a considerable portion of AB that have not underwent a maturation process opening the question if these AB are potentially naturally occurring AB. Intriguingly, NMDARE is across species phenomenon, as NMDARE was causal for the death of polar bear Knut [22] and GluN1 AB are found in other species like dog, cats, rats, mice, baboons and rhesus macaques [23] pinpointing to a higher relevance of these AB.

1.4.2 GluN1 AB in other diseases

Pathognomonic for NMDARE are GluN1 subtype IgG AB in patients' CSF [16]. Despite IgG GluN1 AB subtypes, IgA and IgM are also found in other CNS disorders like schizophrenia [24], dementia [25] and herpes simplex encephalitis [26]. Another study proved the relevance of other GluN1-AB in other diseases (e.g. hypertension, diabetes, etc.) irrespective of immunoglobulin class or epitope [27], indicating that all subtypes of GluN1 AB have pathogenic potential.

1.4.2 GRIN1 mutation

Besides AB-mediated hypofunction, NMDAR functionality can be impaired by mutations in the GRIN1 gene, encoding for GluN1, the essential subunit for NMDAR formation. Besides biparental origin, most GRIN1-mutations develop de novo [28]. The majority of mutations are found within the transmembrane domain of GluN1 causing

loss of function of the receptor. These mutations induce a profound developmental delay with intellectual disabilities in all children, often accompanied by lack of speech, epileptic seizures (in 2/3 of investigated cases), muscle hypotonia and many more [28]. Homozygous biparental mutations were found in two family cases, causing neonatal death in three siblings due to epileptic seizures and were associated with autism spectrum disorders (ASD) in another family [28].

1.4.3 Animal models of NMDAR hypofunction

NMDAR hypofunction is postulated to contribute to the etiology of neurological disorders like schizophrenia, developmental disorders, and ASD [29]. A short summary of animal models based on NMDAR hypofunction is giving in Table 1.

Table 1: Overview of animal models of NMDAR hypofunction

Model	Outcome	Related to	Reference
GluN1 mutant mice	Early neonatal death	Autonomic dysfunction	[30, 31]
Acute application of PCP in rats	+ Stereotypic behavior Social interactions ↓ + Cognitive deficits Pre-pulse inhibition↓	Schizophrenia	[32-34]
Transgenic mice expressing 5% of physiological GluN1-levels	Locomotor activity ↑ +Stereotypic behavior Social, sexual interactions ↓	Schizophrenia	[35]
Chronic application of MK-801 to rat pups from P7-10	Working memory ↓ Cognitive flexibility ↓ Locomotor activity not altered	Schizophrenia	[36]
Transgenic mice expressing 5-10% of physiological GluN1-levels	Locomotor activity not altered Auditory and visual ERP↑ Social interactions ↓ Anxiety-behavior ↓	Schizophrenia	[37]
Transgenic mice expressing 5% of physiological GluN1-levels	Locomotor activity ↑ + Stereotypic behavior + Self-injuries Social interactions ↓ Altered ultrasonic vocalization Pre-pulse inhibition↓	ASD	[38]
***Shank2* mutant mice with NMDAR hypofunction**	Social interactions ↓ + Stereotypic behavior	ASD	[39]
Transgenic mice, GluN1 point mutation	Neonatal death↑ Growth retardation Activity ↓ Poor righting reflex	Developmental disturbances	[40]
Cortical application of MK-801 in P0 rats	Cortical layer misformation Altered electrophysiologial properties	Developmental disturbances	[41]

ASD = autism spectrum disorders; ERP = event-related potentials; MK-801 = Dizocilpine (NMDAR antagonist PCP = phencyclidine (NMDAR antagonist)

1.5 The role of NMDAR during development

1.5.1 Neuronal migration

Neuronal migration is a process during early stages of development crucial for correct positioning of neurons. In the cerebral cortex, postmitotic neuronal cells migrate from the ventricular zone along glial fibers in an “inside-out” fashion with early-born neurons situated deep in the cortex [14]. Experiments investigating the role of NMDAR in context of granular cell migration in mouse cerebellum slice preparations by specific NMDAR blockage revealed dose-dependent decrease of migration that was absent by blockage of other receptors involved in migration ($GABAR_{A/B}$, AMPAR, kainate

receptors) [42]. Surprisingly, neocortical development of GluN1 knockout mice was not affected preterm due to compensation mechanisms that allowed sufficient Ca^{2+} influx [43]. But if MK-801 – an NMDAR antagonist- was applied intracranially during corticogenesis in the developing rat brain, cortical lamination was massively disturbed, proofing toxic effects of acute NMDAR hypofunction during development [41].

1.5.2 Axonal and dendritic arbor elaboration

Mainly studies related to investigation of the sensory system could delineate the role of NMDAR in axonal and dendritic arbor elaboration [44]. E.g. *in vivo* studies in rats using NMDAR antagonists MK-801 and APV revealed an essential role of NMDAR in topographic ordering of retinal projections, as treated neonates had aberrant axons that arborized at incorrect sites [45]. This map formation is characterized by initial overlapping of axons and NMDAR-mediated elimination of branches from inappropriate areas by potential simultaneous firing and retrograde messengers (reviewed in [44]).

Dendritic growth is based on numerous decisions of spatiotemporal arborization of dendrites. As this event is also dependent on synaptic activity, NMDAR are crucial for proper dendritic arbor elaboration. They facilitate: i. Stabilization of actin-skeleton of dendritic filopdia, ii. Recruitment of AMPAR to stabilize spines, iii. Activation of protein synthesis for refinement. NMDAR-mediated arborization is also age-dependent as e.g. a downstream kinase of NMDAR Ca^{2+}/calmodulin-dependent protein kinase II (CaMKII) is minor expressed in immature but highly expressed in mature neurons where its activation stops dendritic growth and thereby stabilizes the dendritic spine (reviewed in [44]).

1.5.3 Neuronal survival

When applied to developing and mature spinal cord neuronal cultures, NMDAR antagonist increase neuronal death only in young neurons, indicating a major role for neuronal survival during development mediated by NMDAR [46]. Further studies associated neuroprotective effects with several down-stream pathways involving anti-apoptotic effects of phosphatidyl inositol 3-kinase (PI3K) dependent pathway, activation of Ca^{2+}/calmodulin-dependent protein (CaM) kinase-cAMP response element binding protein (CREB) which induces expression of brain-derived neurotrophic factor (BDNF) and repression of forkhead box protein O (FOXO) that contributes to oxidative stress-induced cell death (reviewed in [47]).

1.5.4 Development of glutamatergic synapses

Establishment of glutamatergic synapses is an activity-dependent process that is facilitated during early development by NMDAR, AMPAR and $GABA_AR$. Although, principally known for inhibitory synaptic transmission, $GABA_AR$ are excitatory during early development due to increased Cl^- concentrations and expression KCC2 transporter [48]. At the arising synapses, NMDAR are the only glutamatergic receptors present. The lack of AMPAR, result in “silent synapses” as missing AMPAR-mediated depolarization does not repel Mg^{2+} from NMDAR, resulting in inactive NMDAR. It is the GABA-ergic depolarization that mediates NMDAR activation at silent synapses, leading to activation of NMDAR and subsequent insertion of AMPAR [49]. This insertion is seen as a major step towards the establishment of mature glutamatergic synapses.

1.5.5 Functions outside CNS

Eradication of functional NMDAR in GluN1 or GluN2 transgenic mice leads to early neonatal death, indicating that NMDAR perform inalienable functions during post-term development [30, 31]. Although NMDAR are implicated in several aspects of neurodevelopment (see above), gross brain anatomy appeared normal in these mice indicating vital neonatal function for NMDAR besides neuronal migration, axonal and dendritic arbor elaboration, neuronal survival and establishment of glutamatergic synapses. Indeed, NMDAR are also essential components of circuitries responsible for basic functions like normal feeding (suckling behavior)[30, 31, 50], cardiac function [51] and respiration [30, 52]. NMDAR are also found in the kidney, bones thymus [53] and enteric nervous system and contribute to visceral hypersensitivity in humans [54].

1.6 Animal models of gestational AB transfer in neuropsychiatric disorders

The first animal models of gestational transfer were established based on disorders in children that seemed to have a family correlation, but proof of inherited abnormalities was absent. It was hypothesized that maternal autoantibodies are transferred to the fetus during pregnancy, interfering with the respective epitope and finally leading to impaired development of the child, e.g. in autism spectrum disorders [55]. Therefore, animal models of gestational AB transfer were used, to verify this hypothesis. An overview of models in the field of neuropsychiatric disorders is given in Table 2. These studies have proven that maternal transfer of AB during pregnancy causes similar behavioral abnormalities in murine offspring as observed in children, pinpointing to the

harmful potential of maternal autoantibodies. A very recent study (Table 2, 5.) using also a recombinant, human AB comparable to the approach of this study proved that these effects are truly mediated by one AB directed against a distinct epitope and is not due to a mix of various AB (Table 2, 2.-4.) or other components of maternal serum (Table 2, 6.).

Table 2: Animal models of gestational AB transfer in context of neuropsychiatric disorders

	Antibody target	Origin	Anatomical outcome	Behavioral outcome	Related to	Ref.
1.	NR2A/B	Active immunization of the dam	Neurogenesis ↑ Cortical plate width ↓	Cognitive deficits* more male than female mice born	LD	[56]
2.	Fetal brain proteins	Hum, maternal Serum-IgG (pooled)	Glial activation	Locomotor activity↑ Startle response↑ Anxiety-like behavior↑ Sociability↓	ASD	[57]
3.	Fetal brain proteins	Hum, maternal Serum-IgG (pooled)	neurons in CA1 not altered	Delayed motor/sensory development Social interactions↓	ASD	[58]
4.	CASPR2	IgG from CASPR2 encephalitis patients (pooled)	Abnormal lamination of somatosensory CTX Microglial activation PSD95 profiles↓	Social interactions↓ Normal locomotor activity Normal neonatal dev.	n.d.	[59]
5.	CASPR2	mc hum AB	Abnormal cortical dev. dendritic complexity↓ inhibit. neurons in HC↓	Repetitive behavior* Flexible learning↓* Sociability↓ *	ASD	[60]
6.	Purkinje-cells	Hum, maternal Serum	Purkinje cells↓ Cerebellar creatine/choline ↓	exploration↓ motoric performance↓ normal memory function	ND	[61]

*** only observed in male mice; AB = antibody; ASD = autism spectrum disorders; CASPR2 = contactin-associated protein 2; hum = human; IgG = immunoglobulin G; mc = monoclonal; LD = learning disabilities; n.d. = not determined; ND = neurodevelopmental disorder;**

1.7 Overview of developmental features in mice and humans

It is to note that the information given in this introduction is mainly based on studies in rodents as access to human data is limited. To easily access transferability between the used mouse model and humans a comparison of the most important parameters is given in Table 3. It shows that this mouse model is indeed very useful to investigate effects of maternal AB as AB transfer during pregnancy is very similar between humans and mice. Only AB transfer after birth is different and must be considered when interpreting results.

Table 3: Comparison of physiological parameters in mice vs humans

	Mice	Humans
Pregnancy		
1st Trimester	E 0-7.5	GW 1-12
2nd Trimester	E 8-14	GW 13-27
3rd Trimester	E 15-21	GW 28-40
IgG-transfer		
via	yolk sac [62]	placenta [62]
Begin of IgG-transfer	E 11 (2nd trimester) [62]	GW 13 (2nd trimester) [63]
IgG-transfer peak	Postnatal (via BM) [64]	Prenatal (via placenta) [63, 64]
IgG-transfer via BM	Yes	No
NMDAR		
Begin of expression	E14 (2nd trimester)	GW 20 (2nd trimester) [12]*
Expression peak	PNW 3 and adulthood	Pre-term [12]
BBB		
AB penetration	Stops E16.5 [65] At least till P7 (see Figure 10, B)	No data

* no examination before GW 20; AB = antibody; BBB = blood brain barrier; BM = breast milk; PNW = postnatal week

1.8 Hypothesis

During pregnancy, maternal antibodies are transferred to the fetus as a protective mechanism called passive immunity. But also maleficial autoantibodies enter the fetal circulation at a time when blood-brain barrier is not fully established, creating a critical window for anti-neuronal antibodies to compromise proper fetal brain development. Many studies of gestational transfer in mice have proven deleterious effects of various autoantibodies directed against brain proteins (see Table 2) and that anti-GluN1 antibodies lead to NMDAR hypofunction. These circumstances lead to the central research question:

Do maternally transferred GluN1 autoantibodies disturb proper fetal and neonatal NMDAR signaling, leading to neurodevelopmental delays in the offspring with persistent behavioral changes during adulthood?

To address this question, characterization was elaborated by the following steps:

- **Hypothesis 1: GluN1 AB reduce NMDAR in neonatal offspring leading to altered electrophysiological properties**
  - ➔ Verification of AB transfer into circulation and brain parenchyma
  - ➔ Measurement of NMDAR density and evaluation of functional outcome by electrophysiological recordings
- **Hypothesis 2: Immunized mice display reduced bodyweight with impairment in respiration and suckling behavior**
  - ➔ Measurement of physiological parameters like bodyweight, activity, suckling behavior, respiration
  - ➔ Evaluation of contribution of maternal behavior to neonatal phenotype
- **Hypothesis 3: Treated offspring will show delays in neonatal reflexes**
  - ➔ Scoring of neonatal reflexes
- **Hypothesis 4: Fetal and neonatal exposure to GluN1 AB leads to persistent behavioral changes during adulthood**
  - ➔ Investigation of potential behavioral changes in adulthood with paradigms reflecting NMDAR hypofunction
- **Hypothesis 5: Gross brain structure is not affected by AB exposure**
  - ➔ Determination of brain anatomy by MRI volumetry at P0 and old age

2. Materials and methods

2.1 Materials

2.1.1 Chemicals and reagents

Product	Supplier
1,4 Dithiothreitiol	Carl Roth (Karlsruhe, Germany)
2-Methylbutane	Carl Roth (Karlsruhe, Germany)
4',6-Diamidino-2-phenylindole dihydrochloride (DAPI)	Sigma-Aldrich (Saint Louis, MO, USA)
Acrylamide solution 30%	Carl Roth (Karlsruhe, Germany)
Ammonium peroxodisulfate	Carl Roth (Karlsruhe, Germany)
Bovine serum albumin	Carl Roth (Karlsruhe, Germany)
Citric acid	Sigma-Aldrich (Saint Louis, MO, USA)
CruzFluor™488 succinimidylester	Sanat Cruz (Dallas, TX, USA)
Dihydrogen carbonate	Carl Roth (Karlsruhe, Germany)
Disodium hydrogen phosphate	Carl Roth (Karlsruhe, Germany)
Ethanol 70%, 99.8%	Carl Roth (Karlsruhe, Germany)
Femto luminol developing solution	Life technologies (Karlsbad, CA, USA)
FORENE® (Isoflurane)	Abbott (Wiesbaden, Germany)
Glycerol	Carl Roth (Karlsruhe, Germany)
Glycine	Carl Roth (Karlsruhe, Germany)
Immumount	Life technologies (Karlsbad, CA, USA)
Methanol	Carl Roth (Karlsruhe, Germany)
Milk powder	Carl Roth (Karlsruhe, Germany)
Mini-cOmplete ™ proteinase inhibitor tablets	Roche (Basel, Schweiz)
Nitric acid	Carl Roth (Karlsruhe, Germany)
PageBlue™ Protein staining solution	Fisher Scientific (Hampton, NH, USA)
Paraformaldehyd	Carl Roth (Karlsruhe, Germany)
Phenylmethylsulfonyl fluoride (PMSF)	Biochemica (Billingham, UK)
Polyethylenimine (PEI)	Sigma-Aldrich (Saint Louis, MO, USA)
Potassium chloride	Carl Roth (Karlsruhe, Germany)
Potassium dihydrogen phopshate	Carl Roth (Karlsruhe, Germany)
Proteinase inhibitor (cOmplete mini tablets)	Roche (Basel, Switzerland)
SDS Pellets	Carl Roth (Karlsruhe, Germany)
Sepharaose G-beads	GE Healthcare (Little Chalfont, UK)
Sodium azide	SERVA (Heidelberg, Germany)
Sodium chloride	Carl Roth (Karlsruhe, Germany)
Sodium chloride solution (0.9%)	BBraun (Melsungen, Germany)
Tetramethylethylene diamine (TEMED)	Bio-Rad (München, Germany)
Tris(hydroxymethyl)aminomethane	Carl Roth (Karlsruhe, Germany)
Triton-X 100	Th.Geyer (Stuttgart, Germany)
Tween-20	Applichem (Darmstadt, Germany)
Western Lightning developing solution	Perkin Elmer (Waltham, MA, USA)

2.1.2 Cell culture media and supplements

Product	Supplier
Fetal bovine serum, superior	Biochrom (Berlin, Germany)
Dulbecco's MEM, High Glucose, GlutaMax ™ (DMEM)	Life technologies(Karlsbad, CA, USA)
Trypsin/EDTA	Life technologies(Karlsbad, CA, USA)
Poly-L-lysine (PLL)	Biochrom (Berlin, Germany)
Phosphate buffered saline	Life technologies(Karlsbad, CA, USA)
Penicillin/ Streptomycin	Biochrom (Berlin, Germany)
Nutridoma-SP	Roche (Basel, Switzerland)
Non-essential amino acids	Sigma-Aldrich (Saint Louis, MO, USA)

2.1.3 Lab tools and one-way material

Product	Supplier
Biospin Chromatography Spin Column	Bio-Rad (München, Germany)
Coverslips and glass slides	Thermo Fisher Scientific (Waltham, MA, USA)
Syringes and needles	BBraun (Melsungen, Germany)
Cell culture plates and flasks	Corning (New York, NY, USA)
Serological pipettes	Starlab (Hamburg, Germany)
Pipette tips	Starlab (Hamburg, Germany)
15 and 50 mL centrifugation tubes	BD Pharmingen (Heidelberg, Germany)
0.5, 1, 1.5, 2, 5 mL reaction tubes	Eppendorf (Hamburg, Germany)
Nitrocellulose membranes	Bio-Rad (München, Germany)
100 kDa cut-off columns	Merck (Darmstadt, Germany)
Heparinzed collection capillaries	Sarstedt (Nümbrecht, Germany)

2.1.4 Antibodies

2.1.4.1 Primary antibodies

Antibody	Host species	Clonality	Supplier	Reference no	Application	Dilution
Actin	rabbit	pc	Sigma-Aldrich (Saint Louis, MO, USA)	A5060	WB	1:6,000
Homer 1	gp	pc	Synaptic Systems (Göttingen, Germany)	160004	IHC	1:200
CD31	rat	mc	BD Pharmingen (Heidelberg, Germany)	55370	IHC	1:150
Mortalin	ms	mc	NeuroMab (Davis, CA, USA)	75-127	WB	1:6,000
VGLUT1	rb	pc	Synaptic Systems (Göttingen, Germany)	135303	IHC	1:1,000
NMDAR GluN1	rb	mc	Merck KGaA (Darmstadt, Germany)	AB9864R	IHC WB	1:250 1:1,000
Na^+/K^+-ATPase	ms	mc	Abcam (Cambridge, UK)	ab7671	WB	1:1,000

2.1.4.2 Secondary antibodies (anti-IgG)

Reactive species	Host	Conjugation	Supplier	Reference no	Appl.	Dilution
hum	gt	Alexa Fluor 488	Dianova (Hamburg, Germany)	109-545-003	Histo	1:1,000
hum	gt	HRP	Dianova (Hamburg, Germany)	109-035-003	WB	1:6,000
rat	gt	Alexa Fluor 594	Life technologies (Karlsbad, CA, USA)	A1107	Histo	1:1,000
ms	gt	HRP	Dianova (Hamburg, Germany)	115-035-003	WB	1:6,000
gp	gt	Alexa Fluor 568	Life technologies (Karlsbad, CA, USA)	A-11075	Histo	1:1,000
rb	gt	HRP	Vector labs, Peterborough, UK)	PI-1000	WB	1:6,000
rb	gt	Alexa Fluor 488	Dianova (Hamburg, Germany)	111-545-003	Histo	1:1,000
rb	gt	Alexa Fluor 594	Dianova (Hamburg, Germany)	111-585-003	Histo	1:1,000

2.1.5 Kits

Kit	Supplier	Reference no.
Anti-human IgG ELISA	Mabtech(Nacka Strand, Sweden)	3850-1AD-6
Syn-PER™ (synaptosome preparation)	Life technologies(Karlsbad, CA, USA)	87793
Biotinylation kit	Fisher Scientific (Hampton, NH, USA)	QE217779

2.1.6 Software

Software	Application	Provider
Open View software	NMDAR quantification IHC	Noam E. Ziv, Technion-Israel Institute of Technology (Haifa, Israel)
PlotDigitizer	Numeric data extraction	http://plotdigitizer.sourceforge.net/
G*Power	Sample size calculation	http://www.gpower.hhu.de/
R	Statistical analysis	http://www.r-project.org
GraphPad Prism	Statistical analysis	GraphPad Software Inc. (La Jolla, CA, USA)
Adobe Photoshop	Processing of micrographs and WB	Adobe Systems® (San Jose, CA, USA)
Adobe Illustrator	Figure preperation	Adobe Systems® (San Jose, CA, USA)
Microsoft Office	Data processing and writing	Microsoft (Redmond, WA, USA)
ImageQuant TL 7.0	NMDAR quantification WB	GE Healthcare (Little Chalfont, UK)
ImageJ	Competitive assay	http://www.imagej.net
PClamp10 software	Ephys	Molecular Devices (Sunnyvale, CA, USA)
Synaptosoft	Ephys	http://www.synaptosoft.com
Analyze 10.0 software	MRI	AnalyzeDirect Inc. (Overland Park, KS, United States).
MATLAB	MRI	The MathWorks Inc. (Natick, MA, USA)
Viewer 3	Behavioral tests	Bioserve (Mainz, Germany)
CLEVERSYS HCS-software	Behavioral tests	CLEVERSYS GmbH (Entlebuch, Switzerland)

2.2 Methods

2.2.1 Animal experiments

All animal experiments were performed in accordance to the institutional guidelines and were approved by the local ethics committee (Landesamt für Gesundheit und Soziales, Berlin) under the license number G0175/15 and T0007/14. C57BL/6J mice (Forschungseinrichtung für Experimentelle Medizin, Berlin) were housed in individually ventilated cages with max. 5 animals per cage in a 12:12 light/dark cycle with lights on at 6:00 am. Pregnant dams arrived at research facility at gestational day 11 and were single-housed. All animals had *ad libitum* access to food and water and cages were provided with nesting material and a house. For behavioral assessment, animals were transferred to the Behavioral unit within the same building one week prior to testing.

Pregnant dams were intraperitoneally injected at gestational day E13 and E17 with 240 µg purified human monoclonal IgG1 GluN1 AB generated from a female NMDARE-patient (#003-102) in sterile phosphate-buffered saline (PBS, pH 7.4, life technologies, #10010023) or a non-reactive isotype-matched control AB (#mGo53). These AB have

been extensively characterized in previous studies [21] and cross the placenta/yolk sac with highest affinity [62].

Offspring was investigated for AB transfer and AB-mediated effects at different time points of their development. For AB distribution animals were sacrificed at E19, postnatal day (P) 0, P7 and P14. Also, for blood pH analysis, MRI, NMDAR Quantification and electrophysiological recordings animals had to be killed at P0 or P0 and P7, respectively. For developmental scoring, assessment of mortality, bodyweight, activity recordings, MRI and behavioral profile, animals reached adulthood. Therefore, data results from different litters.

2.2.2 Production of human monoclonal antibodies

The following method of generating human monoclonal GluN1 AB (#003-102, #007-168) from cerebral spinal fluid (CSF)-derived AB-secreting cell or memory B cell from two female NMDARE patients during acute phase was established by Dr. med. Jakob Kreye (DZNE, Berlin) [21]. In principle, after FACS sorting of CSF-derived AB-secreting cells and memory B cells, mRNA of single cells was converted into cDNA using a reverse transcriptase reaction. Afterwards, the variable immunoglobulin regions for heavy and light chains were amplified separately and their sequence analyzed. PCR products of the heavy and the matching light chains genes were cloned into a vector with the respective constant immunoglobulin regions, a cytomegalovirus promotor and ampicillin resistance gene. Production of human monoclonal AB was facilitated by transient transfection of human embryonic kidney (HEK293T) cells at 60-80% confluence. HEK293T cells were maintained in 150cm^2 flasks in High Glucose (4.5 g/L) Dulbecco's modified Eagle medium with GlutaMax ™ (DMEM, life technologies #31966-047) supplemented with 10% heat-inactivated fetal bovine serum (FBS superior, Biochrom #S0615), non-essential amino acids (Sigma, #M7145-100ML) and 100 U/mL penicillin/100 µg/mL streptomycin (Biochrom, #A2212). 1 hour prior to transfection, cell medium was changed to serum-free DMEM supplemented with 1% Nutridoma-SP (Roche, #11011375001) and 100 U/mL penicillin/100 µg/mL streptomycin. For transfection of one 150 cm^2 flask, 12.5 µg of each heavy and light chain plasmid was mixed with 125 µL polyethylenimine (PEI, 0.6 g/L, Sigma-Aldrich #408727-100ML) in 1.25 mL sterile 0.9% sodium chloride solution (BBraun, #2350748). Supernatant was harvested at day 3 and 5 after transfection resulting in 50 mL supernatant per flask. For one batch, usually 15 flasks were transfected

resulting in app. 7.5 mL purified AB in PBS with average concentration of 900 -1100 µg/mL.

For purification, cells and debris were removed by centrifugation and cleared supernatant was incubated with 2 µL Protein G Sepharose® beads (GE-healthcare, # 17-0618-01) per mL (100 µL/per transfected 150 cm^2 flasks= total of 1.5 mL) at 4°C overnight in an over-top shaker. Next day, samples were centrifuged at 4,000 g, 10 min to remove supernatant from beads. For 1.5 mL beads, 9 chromatography spin columns (Bio-Rad, # 732-6008) were equilibrated with PBS and beads equally transferred. After washing twice with PBS, AB were eluted in two fractions with 400 µL elution buffer (0.1 M sodium citrate, pH 2.7), neutralized with 40 µL 1 M TRIS-buffer (pH 8.8) per tube. Both fractions were merged and dialyzed against PBS at 4°C overnight. AB concentrations were determined by anti-hum IgG enzyme-linked immunosorbent assay (ELISA) according to manufacturer's instructions (Mabtech) with a developing time of 16-18 min. AB quality and reactivity of each batch was verified via sodium dodecyl sulfate polyacrylamide gel electrophoresis (SDS-PAGE) with subsequent protein staining (PageBlue™, Thermo Scientific, #24620) and staining on GluN1-transfected HEK cells (see method 2.2.7) and on murine brain sections (see method 2.2.8).

2.2.3 Fetal antibody distribution (brain)

Whole embryos (E19) were frozen in ice-cold (-35°C) 2-methylbutane (Roth, #3972.1) and stored at -80°C. 20 µm thick whole-embryo sections were cut, blocked with blocking solution (BS) containing 5% normal goat serum (NGS, Sigma-Aldrich, #H1270) and 2% bovine serum albumin (BSA, Roth, #T844.2) in PBS (137 mM NaCl, 2.7 mM KCl, 10 mM Na_2HPO_4, 1.8 mM KH_2PO_4) for 30 min and stained for VGLUT1 (rabbit-anti-VGLUT1, 1:1,000, Synaptic Systems, #135303) or CD31 (rat-anti-CD31, 1:150, BD, #55370) overnight. Next day, sections were washed with PBS and incubated with secondary AB gt-anti-hum-488 (1:1,000, Dianova, # 109-545-003) to detect injected human AB and gt-anti-rabbit-658 (1:1,000, Life Technologies, #A11036) or gt-anti-rat-594 (1:1,000, Life Technologies, #A11077) for 2h at RT. After washing with PBS, whole sections were mounted with Immumount (Thermo Fisher, #9990402). On the following day, high-resolution epifluorescence tile scans of the whole hippocampus of each specimen were acquired by Mariya Chayka (DZNE Berlin)

with an Inverted Leica DMI8 SPE microscope using 63x Advanced Correction System objective and merged using Leica Application Suite X software.

2.2.4 Neonatal antibody kinetics (serum)

Pups at different age (P0, P7, P10 and P14) were decapitated and trunk blood was collected and coagulated for 1h at RT. Serum was obtained by centrifugation at 340 x g for 10 min at RT. For anti-hum IgG ELISA, neonatal serum was diluted 1:50. Identically obtained maternal serum was diluted 1:100 and 1:20.

2.2.5 IgG Extraction from mouse brain

Brain-bound IgG was extracted from P0 and P7 pups via an acid-based protocol [20] which was modified by Mariya Chayka (DZNE, Berlin). Therefore, brains from P0 pups were homogenized in 6 mL PBS with proteinase inhibitor (PBS-PI, cOmplete mini, Roche, #11836170001) and from P7 pups in 10 mL PBS-PI. Of both preparations, 6 mL was further processed by centrifugation at 4,969 x g for 5 min at 4°C. Resulting pellet was resuspended in 1 mL PBS-PI and centrifuged at 16,000 x g for 5 min at 4°C. Supernatant was discarded and pellet resuspended in 400 µL PBS-PI and repeated twice. In last washing step, pellet was resuspended in 300 µL. After centrifugation, supernatant served as “pre-extraction fraction” (PEF) which should be free of unbound IgG. Remaining pellet was dissolved in 258 µL of sodium-citrate buffer (0.1M, pH 2.7) and incubated for 5 min at RT. After centrifugation at 16,000 x g for 5 min at 4°C, supernatant was neutralized with 42 µL 1.5 M TRIS-buffer (pH 8.8) resulting in extraction fraction (EXF) containing only brain-bound IgG.

2.2.6 ELISA quantification of GluN1-reactive AB

Quantification of GluN1-reactive AB in mouse brain IgG extracts was facilitated in 96-well plates containing the aminoterminal domain (ATD) of GluN1. This ELISA was established and performed by Dr. rer. nat. Hans-Christian Kornau (DZNE, Berlin). In comparison to routine cell-based assay it enables highly sensitive quantification of GluN1-specific concentrations. Wells were coated with donkey-anti-rabbit IgG (20 µg/mL, Dianova, #711-005-152) overnight at 4°C. Next day, after blocking with 2% BSA in PBS/0.05% Tween-20 (PBS-T) at RT, supernatants of HEK293 cells expressing a fusion protein of rabbit Fc and amino acids 1-400 of the human GluN1 were added. IgG extracts (see 2.2.5) were diluted 1:25 or 1:100 in 0.4% BSA-PBS/T and added in duplicates. Plates were washed with PBS-T and incubated with horseradish peroxidase (HRP)-conjugated donkey-anti-human IgG (1:5,000, Dianova,

#709-035-149). After thorough washing, HRP activity was measured using 1-Step Ultra TMB-ELISA substrate (Thermo Fisher, # 34028) and an iMark microplate reader (Bio-Rad). To calculate concentrations of GluN1-reactive AB, a calibration curve with purified #003-102 at 0-3.2 ng/mL was generated.

2.2.7 GluN1 cell assay

HEK293T cells were seeded at a density of 30,000 cells/coverslip on nitric acid-treated and poly-L-lysine-coated 12 mm coverslips (Thermo Fisher, #P231.1) in 24-well plate one day before transfection. Next day, cells were transiently transfected with 1 µg pBud-GRIN1 plasmid [22], 5 µL PEI (0.6 g/L) and 94 µL sterile 0.9% sodium chloride solution per well. After 48 h, coverslips were fixed with ice-cold methanol for 3 min at -20°C. Cells were washed in PBS and blocked for 30 min. Serum, human mc AB or IgG-extracts were diluted in BS and incubated with the cells overnight at 4°C. GluN1 was stained simultaneously with rb-anti-GluN1 (1:250, Merck, #AB9864R). Next day, cells were washed and incubated with respective secondary AB (see 2.1.4.2) for 2h at RT. Again, cells were washed, nuclei stained for 5 min with 4′,6-diamidino-2-phenylindole (DAPI 1µg/mL, Roth, # 6843.1), washed and mounted with Immumount.

2.2.8 Staining of unfixed murine brain sections

In order to characterize NMDAR reactivity of monoclonal AB, 20 µm mouse brain sections of unfixed tissue were blocked with BS for 30 min and incubated with respective human monoclonal AB (#003-102 1µg/mL, #007-168 10 µg/mL) overnight. Next day, sections were washed in PBS and incubated with secondary AB gt-anti-hum-488 (1:1,000, Dianova, # 109-545-003) for 2h at RT. Afterwards sections were washed again and mounted with Immumount.

2.2.9 Quantification of GluN1 protein and detection of human IgG in neonatal brains with Western Blot analysis

Three fractions were quantified for GluN1 density: Synaptosomes (compartment of pre- and post-synapse), cell membrane fraction and total cell fraction (without nuclear fraction). All steps were performed with pre-cooled solutions and equipment on ice. For synaptosomal preperation brains were weighed (P0 ~100 mg, P7 ~300 mg) and homogenized with 10x volume of SynPer™-reagent (Thermo Fisher, #87793) supplemented with PI in a Teflon-glas-douncer with 10 slow strokes. Homogenates were transferred in an Eppendorf-tube and cleared from debris and nuclei by

centrifugation at 1,200 x g, 10 min. Supernatant was centrifuged at 15,000 x g for 20 min. Resulting pellet was resuspended in 100 µL 2x sample buffer (SB, prepared out of 4x SB: 40% glycerol, 9.2% SDS, 122 mM TRIS, 0.01% Bromphenol Blue, 0.32 M Dithiothreitol (DTT)) and 30 µL loaded on a 8% polyacrylamide gel (P0) or resuspended in 300 µL 2x SB and 5 µL loaded (P7). Samples from CTL- and GluN1 AB-treated animals were loaded in an alternating manner.

For preparation of total cell and membrane fractions brains were homogenized in 10x volume of homogenization buffer (0.32 M Sucrose, 10 mM HEPES pH 7.4, 2 mM EDTA, in PBS) supplemented with PI. After centrifugation at 1,000 x g for 10 min, supernatant was transferred into a new tube and an aliquot was kept as total cell fraction mixed with 2x SB. To exclude mitochondria, lysosomes and peroxisomes, remainder was centrifuged at 10,000 x g for 15 min. Supernatant was ultracentrifuged at ~100,000 x g (50.000 rpm TLA-55 rotor) for 60 min obtaining a pellet containing mainly the plasma membrane. Pellet was dissolved in 100 µL (P0) or 300 µL (P7) 2x SB. Samples were loaded in an alternating manner on a 8% SDS-Gel (P0: MF=30 µL, TCF= 20µL; P7: MF =20 µL, TCF=20 µL). 8% polyacrylamide gel was prepared by casting a resolving gel (for 1 gel: 2.4 mL H_20, 1.3 mL 30% acrylamide (Roth, #A124.1), 1.3 mL resolving gel buffer (1.5M Tris/HCl; 0,4% SDS, pH 8.8), 50 µL 10% SDS, 50 µL 10% ammonium peroxydisulfate (APS, Roth, #9592.3) mixed and 3 µL Tetramethylethylenediamine (TEMED, Bio-Rad, #161-0801) added for starting polymerization) and then a stacking gel (for 1 gel: 1.7 mL H_20, 415 µL 30% acrylamide, 315 µL stacking gel buffer (0.5M Tris/HCl; 0,4% SDS, pH 6.8), 25 µL 10% SDS, 25 µL 10% APS mixed and 2.5 µL TEMED) casted on top of resolving gel. Proteins were separated via SDS- polyacrylamide gel electrophoresis (PAGE) in runningbuffer (192 mM Glycine, 25 mM TRIS, 0.1% SDS, pH 8.3) for 30 min at 70V and then app. 1h at 130V. Gels were transferred on 0.2 µm nitrocellulose membranes (Bio-Rad, #1620112) via Trans-blot® Turbo System (Bio-Rad) for 12 min with “High MW transfer” program. Blots were washed in TRIS buffered saline solution (TBS, 20 mM TRIS, 150 mM NaCl) with 0.1% Tween-20 (TBS-T) and protein transfer was verified by incubation with a 10% Ponceau-Red solution.

After intense washing, membranes were blocked in TBS-T containing 5% milk powder (sigma, #70166-500G) and consecutively incubated with 1. rabbit-GluN1 (1:1,000, Merck, #AB9864) overnight and secondary goat-α-rabbit-HRP (1:6,000, Vector labs,

#PI-1000) the next day for 2h at RT with intensive washing steps with TBS-T in between. Blots were developed with Western Lightning® solution (Perkin Elmer) and recorded with luminescence-based ImageQuant® LAS 400 mini. 2. Blots were incubated with AB for reference proteins (Synaptosomal and total cell fraction: mouse-anti-Mortalin, 1:5,000, Neuromab #75-217; membrane fraction: rabbit-anti-ß-Actin, 1:3,000, Sigma Aldrich #A5060) overnight. Adding 0.05% NaN_3 to AB solution eradicated HRP-signal from previous secondary AB. On the next day, respective secondary AB (1:6,000, goat-anti-mouse-HRP, Dianova, #115-035-003; goat-anti-rabbit-HRP, Vector labs, #PI-1000) was applied for 2h at RT to the blots and developed as stated above.

Last recoding before oversaturation of the blots was used for quantification with ImageQuant®. Protein intensities were calculated as area under the curve and background was subtracted automatically. As intensities vary between blots, individual protein signal was divided by the mean of all samples. Afterwards, a ratio of GluN1 protein expression to reference protein was calculated and compared.

For detection of hum IgG within neonatal brain, homogenates of synaptsomes were analyzed like described above and membranes incubated with goat-anti-hum-HRP (1:6,000, Dianova, # 109-035-003) overnight and developed the next day.

2.2.10 Quantification of GluN1 protein expression with immunohistochemistry

2.2.10.1 Competitive assay of GluN1-reactive AB #003-102 and #007-168

As previous stainings revealed that human monoclonal GluN1 AB are more sensitive in unfixed tissue than any commercial AB used, we decided to use another human GluN1 AB produced in our lab on neonatal sections that show partially low NMDAR expression (P0 pups). As a prequisite for GluN1 quantification, binding to the same epitope as the injected AB #003-102 had to be excluded. Therefore, a competitive assay with both AB was performed on murine sections. In principle, AB were labeled with CruzFluor™488 succinimidylester (10 mg/mL, SantaCruz, #sc-362617, 8.4 µL for 1 mg AB for 1h, RT) and residual fluorochrome was removed by 100 kDa cut-off columns (Amicon®, # Z677906-24EA). For assay verification, murine brain sections were incubated with a fixed concentration of labeled AB (1 µg/mL for #003-102 and 10 µg/mL for #007-168) adding increasing concentrations of the identical unlabeled AB resulting competitive displacement (Figure 3: A-E, F-J). Afterwards, labeled AB were incubated with increasing concentrations of the other AB, not showing displacement

(Figure 3: K-O, P-T). This suggests different epitope binding of these human monoclonal AB and justifies use of #007-168 for GluN1 quantification. Quantification of signal intensity was performed with ImageJ (Figure 3, U,V) by calculating the mean of two squares from hippocampal *Stratum radiatum* (Figure 3, A) and subtracting background from comparable juxta-hippocampal regions (Figure 3, A).

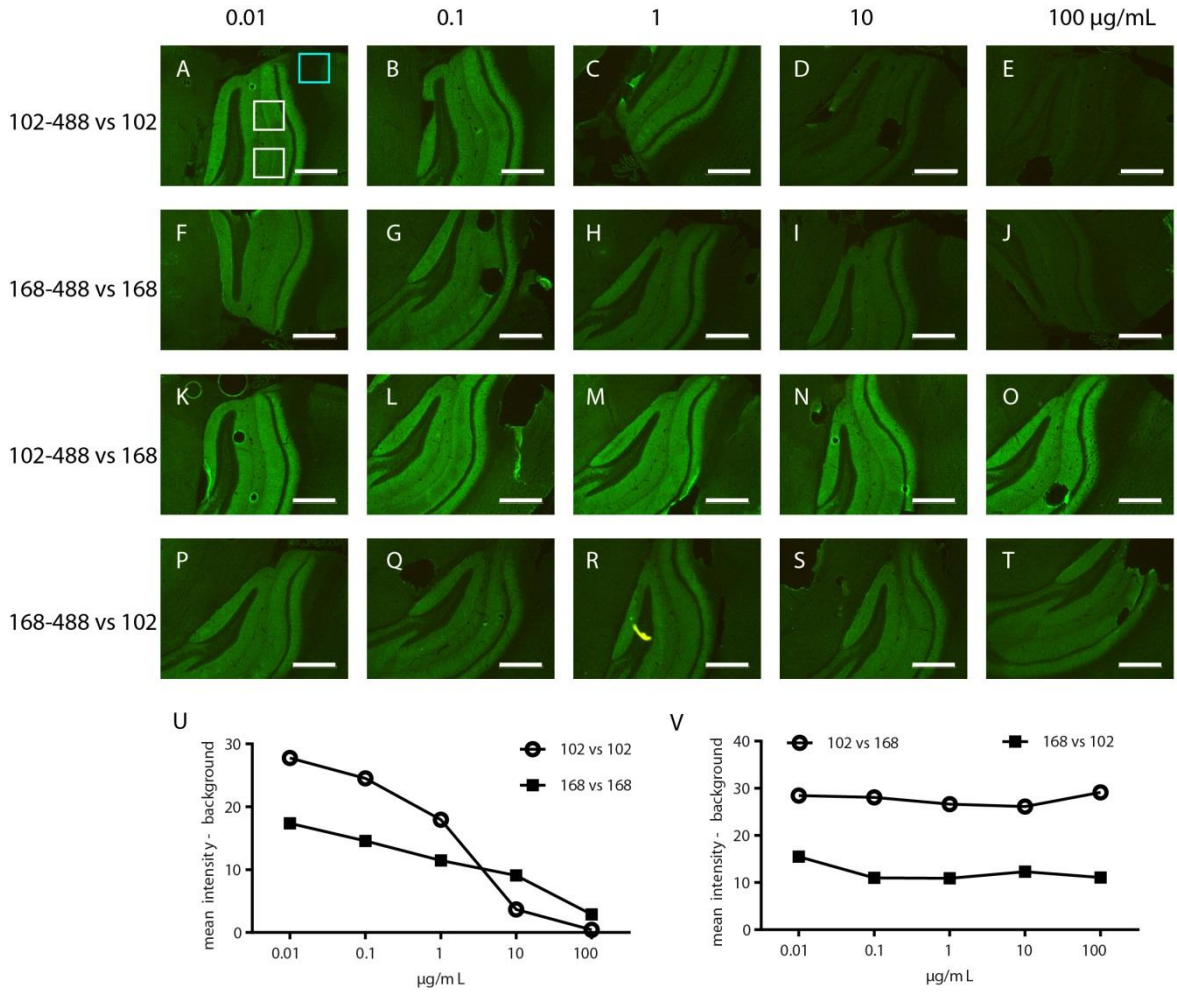

Figure 3: Competitive assay of GluN1-reactive human AB #003-102 and #007-168.
Both AB were labeled with Alexa-Fluor 488 and epitope evaluation was assessed by verification of AB displacement by reduction in signal intensity on murine brain sections. Validation of assay was performed by adding increasing concentrations of the same unlabeled AB (#003-102 **A-E**; #007-168 **F-J**), leading to reduction in signal intensity with increasing concentrations. This reduction was absent when the other AB was added (#007-168 to #003-102-488 **K-O**; #003-102 to #007-168-488 **P-T**). Quantification was performed with ImageJ by calculating the mean of two squares within the hippocampus (**A**, white squares) and subtraction of background signal (**A**, turquoise square) revealing positive displacement by identical AB (**U**) and absent displacement by the other AB (**V**). Scale bar=100µm.

For quantification of GluN1 in neonatal brain sections, P0 or P7 pups were decapitated and brains were frozen in ice-cold (-35°C) 2-methylbutane and stored at -80°C. 20 µm thick sections were cut in a cryostat, air-dried and stored at -80°C until stained. For GluN1 quantification, human monoclonal AB #007-168 was biotinylated according to manufacturer's protocol (Thermo Fisher, #QE217779). Sections were thawed at 4°C, blocked with BS for 30 min and incubated with 15 µg/mL #007-168-Biot for GluN1 detection and Homer-1 (1:200, Synaptic Systems, #160004) as a synaptic marker, in BS for 2 days at 4°C. On the third day, sections were washed 3x times for 5 min in PBS without agitation. Secondary AB gtαgp-568 (1:1000, Invitrogen, #A-11075) and Streptavidin-488 (Invitrogen, #A-32360) was diluted in PBS with 2% BSA for 2h, RT. Again, sections were washed three times and mounted with Immumount, dried for one hour at RT and then stored at 4°C. Two pictures (Z-stacks: 16 x 0.3µm) from CA3 region were with a Zeiss Axio Observer (Z1 with Andor spinning disc and cobolt, omricron, i-beam laser) using a 63x 1.4 NA Plan-Apochromat oil objective and an iXon ultra (Andor, Belfast, UK) camera controlled by iQ software (Andor, Belfast, UK). Pictures were taken from 3 individuals of at least 3 different litters, starting with reference protein Homer-1. For analysis investigator was blinded to treatment allocation. First, Homer-1-positive synaptic clusters were selected manually creating a "cluster-mask" that was transferred to micrograph of GluN1 staining and fluorescence intensities for human GluN1 AB #007-168 were calculated automatically for each site selected and corrected for background fluorescence using Open View software (provided by Noam E. Ziv, Technion-Israel Institute of Technology, Haifa, Israel via Prof. Graig Garner, DZNE, Berlin). Overlapping punctae of Homer-1 and human GluN1 were counted and displayed as ratio of co-localized to synaptic punctae. The basic protocol for quantification was modified, and all quantifications were performed by Mariya Chayka (DZNE, Berlin).

2.2.11 Electrophysiological recordings

Whole-cell patch clamp recordings were performed on acute slices in order to assess electrophysiological properties. Preparation, recordings and data analysis were performed by Larissa Kraus, M.Sc. under supervision of Dr. med. Pawel Fidzinski (Experimental Neurology, Charité, Berlin). Therefore, P0 or P7 pups were decapitated and horizontal slices (350 µm) from hippocampus were cut with a vibratome (Leica VT1200S) in ice-cold artificial cerebrospinal fluid (aCSF I: 87 mM NaCl, 1.25 mM NaH_2PO_4, 0.5 mM $CaCl_2$, 2.5 mM KCl, 7 mM MgCl2, 26 mM $NaHCO_3$, 75 mM sucrose,

25 mM glucose). Fresh slices were immediately transferred to a holding chamber at 32-35°C for 30 min filled with aCSF II (129 mM NaCl, 1.25 mM NaH_2PO_4, 1.6 mM $CaCl_2$, 3.0 mM KCl, 1.8 mM $MgSO_4$, 21 mM $NaHCO_3$, 10 mM glucose), followed by incubation at RT until recording. For measurement borosilicate pipettes (1.5 mm outer diameter, Science Products) were pulled with a vertical puller (Narishige, PC-10; 4-6 mΩ) and filled with internal solution containing 125 mM CsCl, 2mM Mg_2Cl, 10 mM HEPES, 2 mM EGTA, 2mM Na2ATP, 0.3 mM NaGTP. Recordings were performed on pyramidal neurons in the CA1 region of the hippocampus. Access resistance did not exceed 20 MΩ and varied less than 20% during all experiments and series resistance compensation was not used. Obtained signals were low-pass filtered at 2 kHz and sampled at 10 kHz by a Digidata 1550 interface and processed by PClamp10 software (Molecular Devices, Sunnyvale, CA, USA). Spontaneous excitatory postsynaptic currents (sEPSC) were recorded at -70mV for at least 4 min. Recordings at +40mV after 50ms reflecting NMDAR-mediated currents did not result in sufficient amounts of traces to perform proper analyses. GABAA-R antagonist SR-95531 was applied to the bath solution (1 µM, Tocris) in order to avoid depolarizing GABA currents. Analysis of sEPSC was performed with MiniAnalysis software (Synaptosoft, http://www.synaptosoft.com).

2.2.12 Determination of blood-pH

Blood pH of newborn pups was measured with an ABL-80 FLEX BASIC blood gas analyzer (Radiometer). Mice were placed in a heating chamber (35°C) to prevent cooling down. For measurement, animal to be tested was decapitated and trunk was collected with a heparinzed collection capillary (SARSTEDT, #19.930.100). Due to insufficient minimal sampling volume (min. 100 µL) for measurement, murine blood volume collected was measured by a scaled capillary and mixed with twice the of heparinzed (5.000 I.E.) 0.09% NaCl solution, resulting in a 30% blood solution. µL was transferred into a new capillary with a pipette. Dilution-mediated effects were assessed beforehand with blood of two adult mice (

Figure 4).

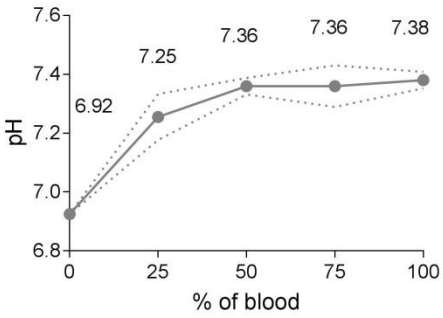

Figure 4: Determination of blood pH in diluted blood samples.
Trunk blood from two adult animals was diluted to different concentrations and blood pH measured with an ABL-80 blood gas analyzer.

2.2.13 Activity measurement

For activity recordings, a transponder was implanted into each animal, sending spatiotemporal information to an ID-sensor-grid underneath the home cage. Twelve-week-old animals were recorded for 14 days. Data was kindly analyzed by Patrick Bey, AOCF, Charité, Berlin).

2.2.14 MRI-based determination of brain volume

Magnetic resonance imaging (MRI) was performed on P0 pups and 10-month old offspring using a 7-Tesla small animal Scanner (7T BioSpec + 1H-Cryoprobe, Bruker, Ettlingen, Germany). By using isoflurane, P0 were euthanized immediately prior to recordings and placed in prone position. Adult animals were anesthetized by isoflurane. Total and hippocampal volume of P0 pups were assessed using high resolution morphological T2-weighed TurboRARE sequence (repetition time/echo time = 4000/34.5 ms, 10 averages, rare factor 8, 36 coronal slices per 0.25 mm, field of view: 12.8x12.8 mm^2, Matrix: 170x170 = inplane resolution of 75x75 μm^2; scan time 14 min). Volumetry of total brain and hippocampus of P0 neonates were performed using Analyze 10.0 software (AnalyzeDirect Inc., Overland Park, KS, United States). For adult mice, a different high resolution morphological T2-weighed TurboRARE sequence was used (repetition time/echo time = 4250/33 ms, 2 averages, rare factor 8, 40 coronal slices per 0.40 mm, field of view: 19.2x19.2 mm^2, Matrix: 192x192 = inplane resolution of 100x100 μm^2; scan time 3m24sec). Volumetry of different regions was performed using a homemade MATLAB toolbox to register mouse brain MR images to the Allen brain atlas [66]. Measurements, data analysis and statistical analysis were performed by Susanne Mueller, Dipl.-Ing., Dr. rer. nat. Stefan Koch and Dr. rer. nat. Philipp Boehm-Sturm (Experimental Neurology, Charité, Berlin)

2.2.15 Neurodevelopmental Scoring

To evaluate the establishment of neonatal reflexes, neonates were scored daily from P3-P12 according to a reduced protocol from Heyser [67]. Animals were transferred to a calm room and acclimated for 30 min. When testing started, dam was transferred in a separate cage. Neonates were scored and transferred to a warm box afterwards to prevent cooling down of pups. First reflex evaluated was righting reflex: animal was placed on the back and latency to turn around on all four paws was recorded. Cut-off time was 30 seconds and animals were put back in their physiological orientation if they failed to turn around. Afterwards, cliff avoidance was evaluated by placing the pups close to an edge of 30 cm elevated platform and latency for the animal to turn around and walk away was recorded. Cut-off time was 30 sec. Third reflex scored was negative geotaxis, where animals were placed head facing downwards on a 30° inclined plane with a rough surface, in order to provide enough grip for the animals. Cut-off time was also 30 seconds and test was stated as successfully performed when animal turned around in a 180° angle. All reflexes were considered established, when all animals of a group performed reflex within cut-off time.

2.2.16 Behavioral assessment

All behavioral tests were performed at the Animal Outcome Core Facility (AOCF) with technical assistance of Melissa Long, B.Sc., and support in project planning and statistical analysis of Dr. rer. nat. Marion Rivalan (AOCF, Charité, Berlin). In order to assess the general health status and morphological phenotype of adult CTL and GluN1-AB treated mice, a modified SHIRPA test was performed with five-week-old animals [68]. All animals displayed a normal phenotype.

2.2.16.1 Social preference in 3-chamber-test

Test for social preference was performed by six-week-old animals in a three-chamber box (60x40x22 cm, Stoelting apparatus). Each chamber was 20x40x22 cm and connected by a closable hole. Animals explored the arena for 10 min before the test started (habituation). Afterwards an empty cage (“object”) and a cage containing an unfamiliar (“stranger”) C57BL/6J mouse (same sex) was placed in one of the side chambers. Allocation of cages was systematically alternated between test animals. Velocity, duration in each chamber and time spent close to the cages was recorded by the video-tracking system Viewer 3 (Bioserve, Mainz, Germany) and analyzed as a ratio of duration interacting with unfamiliar mouse (“stranger”) to empty cage (“object”).

2.2.16.2 Learning and memory recall in Barnes Maze

Test for learning and memory capabilities was performed by seven-week-old mice in a Barnes Maze arena. Mice were trained on a white platform to find a hidden escape box in 1 out of 20 holes for 4 days with 4 trials each day (16 in total) with orientation marks displayed on the wall. Behavior and distance travelled were recorded with Viewer 3 software (Bioserve, Mainz, Germany). Immediately after the animal was placed in the middle of the platform, it was exposed to a white noise stimulus (85 dB), which stopped after escape box was successfully found. Cut-off time were 180 sec during training and 90 sec during testing. After 24 hours and one week respectively, mice were tested for their capabilities of memory recall in one trial for 90 sec. Therefore, platform was divided in four zones and time spend in the correct zone in comparison to total duration was calculated. For evaluation of learning capabilities latency to find the correct hole was analyzed over all 16 test trials.

2.2.16.3 Anxiety-like behavior in Elevated Plus Maze

In order to assess anxiety-like behavior, eight-week-old mice were tested on an Elevated Plus Maze (EPM), white PVC (50x50x53 cm) with 2 open arms and 2 closed arms. Mice were place in the middle crossing and allowed to explore for 5 minutes. Activity in the EPM was tracked and recorded using Viewer 3 software (Bioserve, Mainz, Germany). Visits were recorded manually. Anxiety-like behavior was calculated by duration and visits in and into the open arms

2.2.16.4 Pre-pulse inhibition in Acoustic startle response test

Acoustic startle response test was used to measure pre-pulse inhibition (PPI) in nine-week-old animals. Therefore, mice were individually restrained in small cages to restrict major movements and placed on measuring platforms with high precision sensors in sound-attenuating isolated boxes (TSE systems, Bad Homburg, Germany). Test was based on a protocol from Lipina et al. [69] with five trials per block consisting of white noise (N56dB), acoustic startle (P120dB, 40 ms) and three pre-pulse acoustic startle trials (PP69dB, PP73dB, and PP81dB for 20 ms, 100 ms before acoustic startle of P120dB, 40 ms). After a 10-minute acclimation period, five acoustic startle trials (P120 dB) were applied, followed by 10 blocks of the five pre-pulse trials (PP69 dB-P120 dB; PP73 dB- P120 dB; PP81dB- P120 dB) in pseudorandom order and another five acoustic startle trials (P120 dB). The inter trial intervals were distributed between 12 and 30 seconds. For analysis, general startle reaction (maxG), habituation to

stimulus and PPI was considered. PPI was calculated as: 100- [(mean startle response on acoustic pre-pulse startle stimulus trials/mean startle response alone trials) x 100].

2.2.16.5 Individual behavior in Home Cage Scan-Analysis

In order to detect repetitive behavior or general abnormalities in circadian rhythmicity, animals were individually recorded in their home cage via HomeCageScan (HCS) software (CLEVERSYS GmbH, Entlebuch, Switzerland). Recordings were performed over 23 h (11 h of light phase and 12 h of dark phase), as the hour of setting up the software and ending the test (11 a.m.) was excluded. Among other behaviors recorded, the more relevant behaviors for this study grooming, twitching, consumption (eating and drinking), and sleeping were analyzed.

2.2.16.6 Nest construction behavior

As a robust indicator for general wellbeing and normal brain function, nest construction behavior was analyzed of 12-14-week-old mice. Each mouse was single-housed 24 hours before the test and given nesting material nestlets (5x5 cm squares of pressed white cotton) for habituation. The next two consecutive days, mice nestlets were placed in the middle of each cage and evaluation of nest complexity was scored and the remaining intact nestlet material weighed the next morning. A nest typically consisted of a low pile of bedding with a crater at the top, surrounded by, or sometimes covered with, shredded cotton. Based on the protocol of Deacon et al. [70] nests were scored in 6 complexity types: **0** no visible piling of bedding and no shredded cotton; **1** bedding mound and crater alone, no shredded cotton; **2** bedding mound and crater, cotton shredded around (flat); **3** bedding mound and crater, cotton shredded around to form a crater-shaped nest; **4** bedding mound and crater, cotton shredded around to form a cup-shaped nest; **5** bedding mound and crater, cotton shredded around to form a ball-shaped nest.

2.2.16.7 Motoric performance in the Rotarod test

Eleven-months-old offspring performed a one-day Rotarod test on a rotating rod apparatus (TSE Systems, Bad Homburg, Germany) allowing measurement of 5 mice simultaneously. Basically, the tests assess the motoric abilities my measuring the duration of each animal balancing on an accelerating rotating rod. Animals performed three consecutive trials with maximum time on the rod of 300 sec. In between trials,

animals rested for 15 min. Rotation started at 4 rpm and accelerated to 40 rpm over 300 sec. Afterwards, latency to fall and learning within three trials was analyzed.

2.2.17 Methods to prevent bias

In order avoid methodical bias, different precautions were taken. For injection, pregnant dams were randomly assigned. After weaning, mice of both treatment groups were mixed-housed to avoid litter-based bias. Within all experiments, animals or samples were used in an alternating manner. Investigator was blinded for treatment for MRI measurements including analysis, electrophysiological recordings including analysis, Barnes Maze, Rotarod and GluN1-positive cluster quantification.

For behavioral paradigms, sample size was calculated by a priori power analysis with G*Power (http://www.gpower.hhu.de/) using publicly available data sets and extracted numeric data using Plot Digitizer (http://plotdigitizer.sourceforge.net/).

2.2.18 Statistical analysis

Statistical analyses were planned with support of Klaus Lenz (Institute for Biometrics and Clinical Epidemiology, Charité, Berlin) and performed with GraphPad Prism 7 (GraphPad Software, Inc., La Jolla, CA, USA) and R (http://www.r-project.org). Data are presented as scatter plots with mean±SD or median with 95% confidence intervals an min-max boxplots. Statistical analyses included t-test, ANOVA, repeated measurement ANOVA following Holm-Sidak- or Tukey's multiple comparison test. Mann-Whitney and Kruskal-Wallis tests were used for non-parametric data (mainly data from behavioral assessment) followed by Dunn's multiple comparison. Wilcoxon-test was used to compare total activity of animals, one-sided Fisher's exact test for frequency distribution, Kaplan-Meier log rank test for survival with Bonferroni correction. $P<0.05$ was considered statistically significant.

3. Results

3.1 Study design

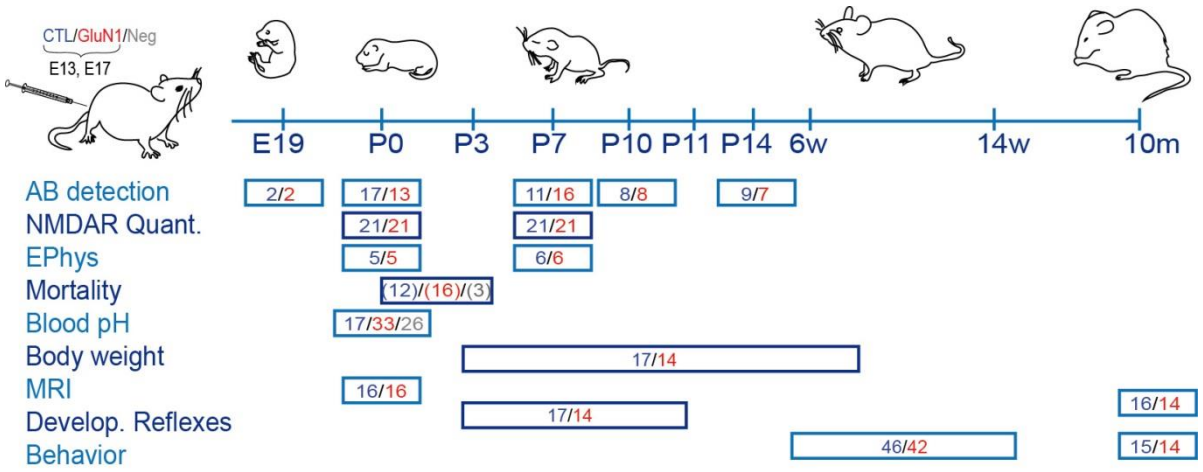

Figure 5: Immunization protocol and assessment of AB-mediated effects in offspring at different developmental stages.
A total of 480 µg of human monoclonal CTL or GluN1 AB were intraperitoneally injected into pregnant dams and different aspects of the hypotheses were evaluated at different developmental stages of the offspring. For detailed description see text. Numbers in rectangles represent number of pups used or litters in brackets, respectively.

Pregnant C57BL/6J were intraperitoneally injected with 240 µg human, monoclonal AB either GluN1 (#003-102) or non-reactive CTL AB (#mGo53) subtype IgG1 on gestational day E13 and E17. As control for human AB treatment, dams were not injected (“Neg”). First, AB transfer and binding was verified at different developmental stages via whole-embryo stainings against human IgG (E19), anti-hum IgG ELISA of neonatal serum (P0, P7, P10, P14) and extraction of bound IgG from neonatal brain tissue (P0, P7) (“AB detection”). Density of NMDAR was quantified to verify NMDAR reduction hypothesis via IHC and analysis of different cell fractions via WB at P0 and P7 (“NMDAR Quantification”). Recordings of spontaneous EPSCs were performed on acute slices from P0 and P7-old pups (“EPhys”) to characterize functional outcome of GluN1 AB-treatment. Survivability was analyzed during early neonatal period (P0-P3, “Mortality”) and blood pH was determined at day of birth (“Blood pH”) to check for respiration status. Bodyweight, as a robust marker for developmental disturbances, was recorded from early neonatal day P3 to adulthood (8 weeks). To detect possibly AB-mediated changes in brain volume, MRI scans of brains were performed on day at birth and on aged offspring (>10 months, “MRI”). Neonatal reflexes were scored from

P3 and P11 (“Develop. Reflexes”), whereas behavioral profile was characterized during adolescence and adulthood with paradigms investigating NMDAR hypofunction and motoric performance (“Behavior”). Adequate maternal behavior and suckling behavior was checked between P0 and P7 (not shown in Figure 5).

3.2 Antibody characterization

In contrast to most other animal models of gestational transfer of anti-neuronal AB (see Table 2) usage of mixed IgG or serum was omitted and a single, human, monoclonal GluN1 AB was used to obtain truly GluN1 AB-mediated effects. The isotype-matched control AB used did not show any reactivity on murine brain sections or in routine cell-based assay using GluN1-transfected HEK cells (Figure 6 A-C) and was non-reactive in other assays [71]. The GluN1 AB used (#003-102) was generated from a female NMDARE patient and shows a typical NMDAR staining pattern in hippocampus (Figure 6, D), cerebellum (Figure 6, E) and on transfected HEK cells (Figure 6, F). This AB has been intensively characterized in previous studies [21], proving strong GluN1 reactivity by reducing NMDAR clusters *in vivo* with subsequently reduced calcium influx [21].

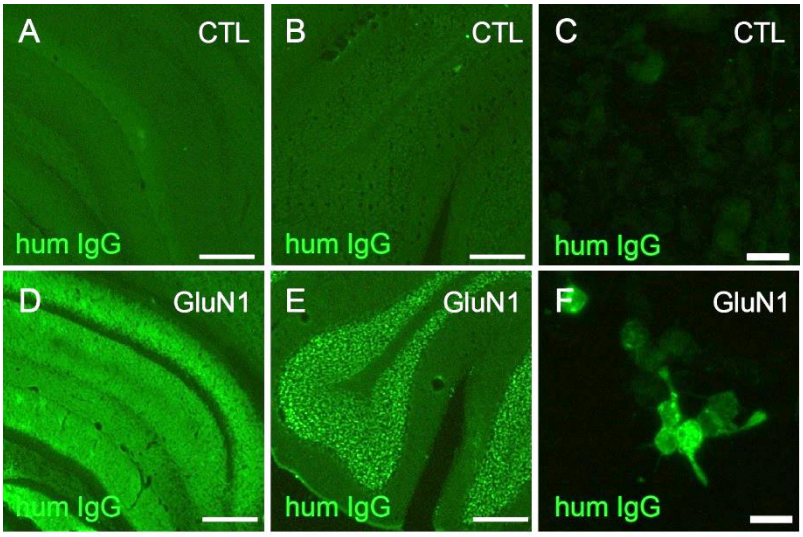

Figure 6: Reactivity of human monoclonal CTL and GluN1 AB on murine brain sections and transfected HEK cells.
CTL AB used for this study (#mGo53) does not show any binding to neither hippocampal region (**A**) nor to cerebellum (**B**). Also no binding is seen to GluN1 in GluN1-transfected HEK cells (**C**). Human monoclonal GluN1 AB (#003-102) binds to the neuropil within the hippocampus (**D**) and to granular cells of the cerebellum (**E**). Also binding to GluN1 on transfected HEK cells is observed (**F**). Scale bars: A, B, D, E = 50µm; C, F = 20 µm.

3.3 Gestational AB transfer

3.3.1 Serum

Verification of maternal transfer of human AB into offspring's circulation revealed elevated levels of serum AB in neonatal circulation compared to AB levels of their respective mothers (Figure 7, A). Detection of neonatal AB-levels over time showed a peak at day of birth for CTL AB-treated neonates, whereas serum levels of GluN1 AB-treated offspring peaked at postnatal day seven. Both groups displayed declining levels with similar concentrations at postnatal day 14. Pregnancy reduced AB-levels in the dams as non-pregnant mice displayed higher AB-levels with half of the AB injected, indicating that a considerable amount of AB is transferred to the offspring (Figure 7, B). On a routine cell-based assay, maternal serum of GluN1 AB-treated dams displayed binding up to a dilution of 1:1,000 (Figure 8, A-E) and neonatal serum 1:5,000 indicating AB-enrichment in the neonates (Figure 8, F-J). Serum of CTL AB-treated dams and neonates did not show any binding to GluN1-transfected HEK cells (Figure 8, K-T).

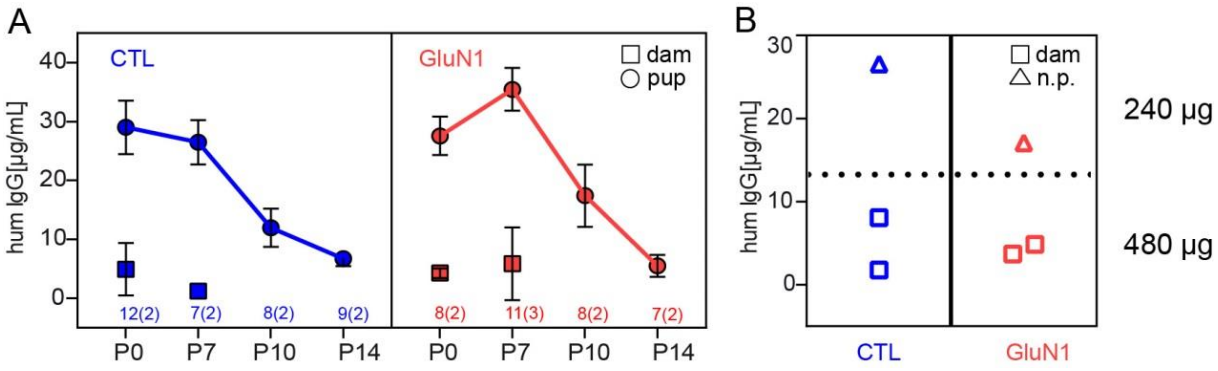

Figure 7: Detection of maternally transferred human AB via anti-human IgG ELISA.
Both CTL and GluN1 AB are successfully transferred and enriched in the neonatal circulation (**A**, squares= dams, circles = pups). Both groups show declining levels until P14. Numbers below data points represent pups and litters (in brackets) used for this experiment. Data is represented as mean±SD. Pregnant dams injected with 480 µg AB display lower levels of serum AB in comparison to non-pregant (n.p.) mice injected with 240 µg AB (**B**, individual data points). Collection of blood samples was time-matched to day of birth of pregnant dams.

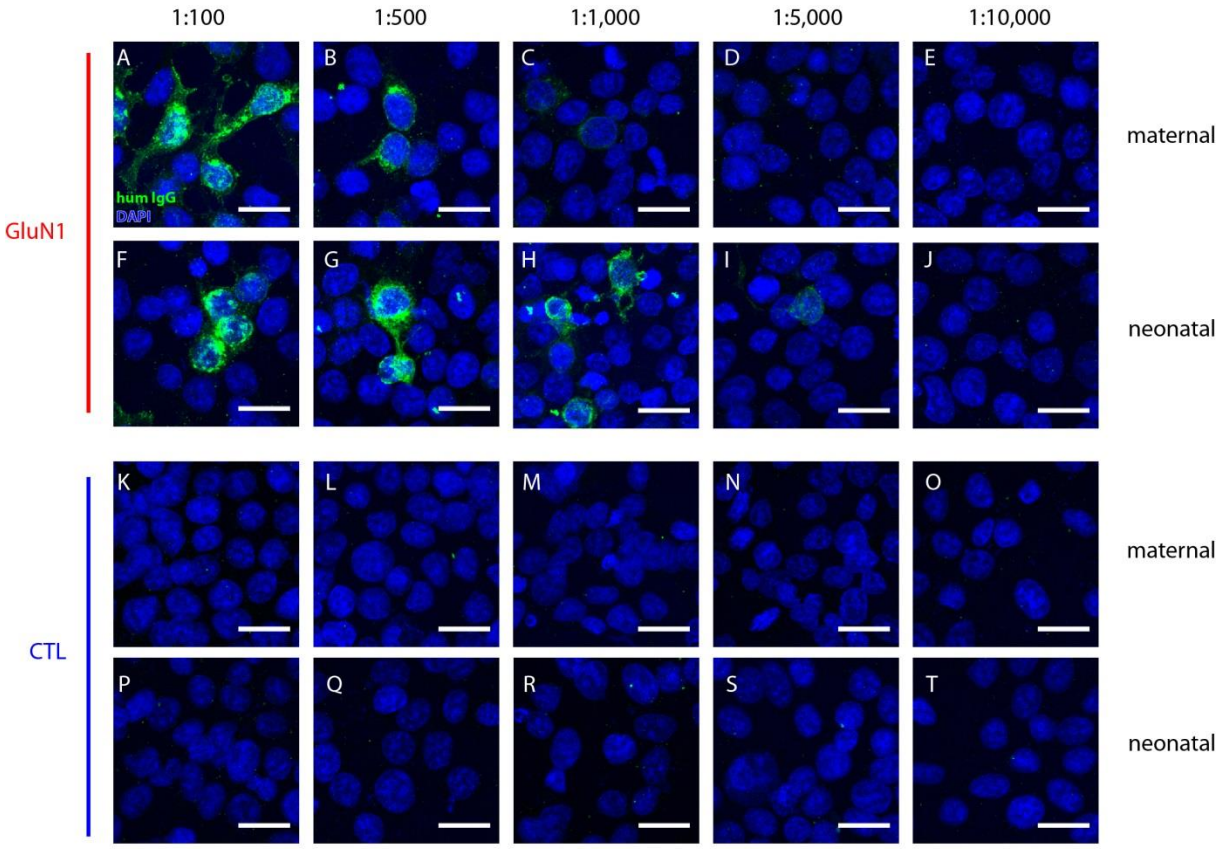

Figure 8: Representative pictures of serum binding of CTL and GluN1 AB-treated dams and neonates to GluN1-transfected HEK cells.

Each row represents dilution steps from 1:100 to 1:10,000 of serum collected at day of birth. Serum AB levels of GluN1 AB-treated dams (**A**-**E**) were detectable at 1:1,000 dilutions (**C**). Serum binding to GluN1 in the respective offspring (**F**-**J**) was detectable at a dilution of 1:5,000 (**F**), indicating AB enrichment in the neonatal circulation. CTL AB-treated dams (**K**-**O**) and neonates (**P**-**T**) lacked serum binding to GluN1-expressing cells.

3.3.2 Brain

As NMDAR are mainly located within the CNS, verification of passage of maternally transferred AB into brain parenchyma of offspring is essential. One approach was to detect localization of human AB within the fetal brain (embryonic day E19) by

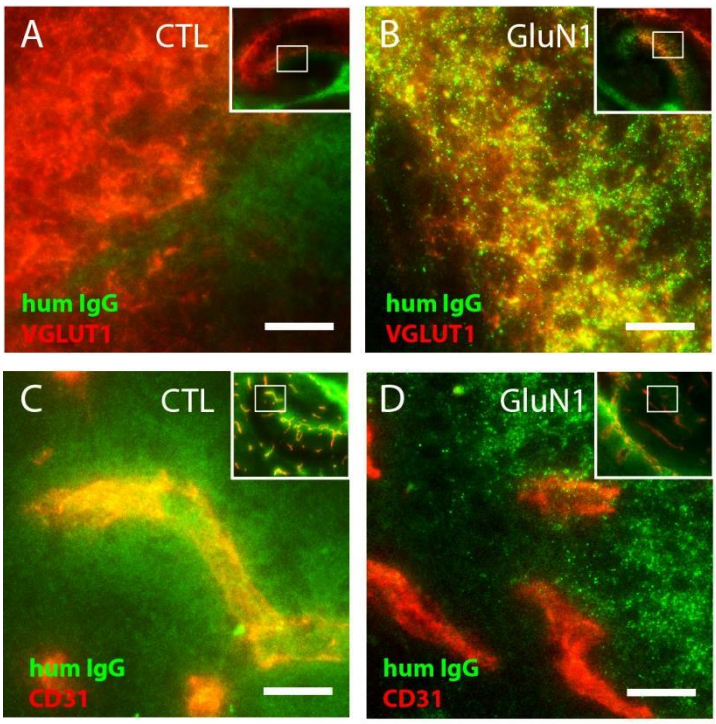

Figure 9: Distribution of maternally transferred human CTL and GluN1 AB within the fetal brain.
Maternally transferred CTL AB (human IgG) does not co-localize with synaptic marker VGLUT1 (**A**) whereas GluN1 AB co-localizes with synaptic marker VGLUT1 (**B**). CTL AB is diffusely located around blood vessels as seen in co-staining with the epithilial marker CD31 (**C**) whereas GluN1 AB penetrates into brain parenchyma (**D**). Inserts show the area of the micrograph in the hippocampus (**A-D**). Scale bars: 100 µm.

immunofluorescence staining. Co-staining with blood vessel marker CD31 and synaptic marker VGLUT1 disclosed different staining patterns for CTL- and GluN1 AB-treated mice in fetal brain tissue. Whereas CTL AB was not localized at synapses (Figure 9, A) and diffusely located around blood vessels (Figure 9, C) maternally transferred GluN1 AB co-localized with synaptic marker VGLUT1 (Figure 9, B) and penetrated into brain parenchyma (Figure 9, D).

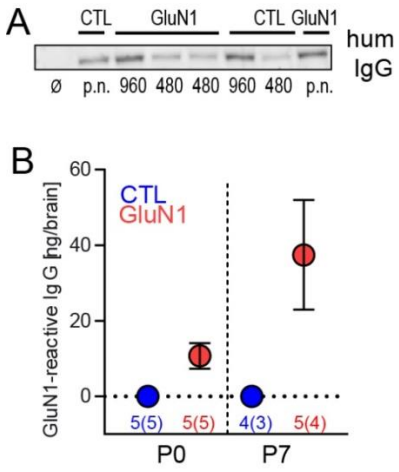

Figure 10: Detection and extraction of human IgG from neonatal brain tissue.
Western blot (cropped) of neonatal brains detected human IgG in both CTL and GluN1 AB-treated animals at different concentrations (**A**, 960 µg per dam; 480 µg; Ø=untreated; p.n.=postnatal injection [480 µg]). Quantification of GluN1-specific AB in brain IgG extracts revealed increasing levels of brain-bound IgG from P0 (mean= 10.7 ng) to P7 (mean= 37.4 ng, mean±SD (**B**). Numbers below data points represent pups and litters (in brackets) used for this experiment.

Presence of human IgG was also verified by Western Blot analysis revealing concentration-dependent transfer (Figure 10, A). In order to detect only brain-bound IgG, acid-based IgG-extraction of neonatal brains at day of birth (P0) and postnatal day seven (P7) was performed. Analyzing these IgG extracts by quantifying exclusively GluN1-reactive AB with ELISA (see 2.2.6) unveiled increased concentrations of brain-bound GluN1 AB at P7 compared to P0 (Figure 10, B). These extracted AB retained their capability to bind to GluN1 as proven by stainings on transfected HEK cells (Figure 11).

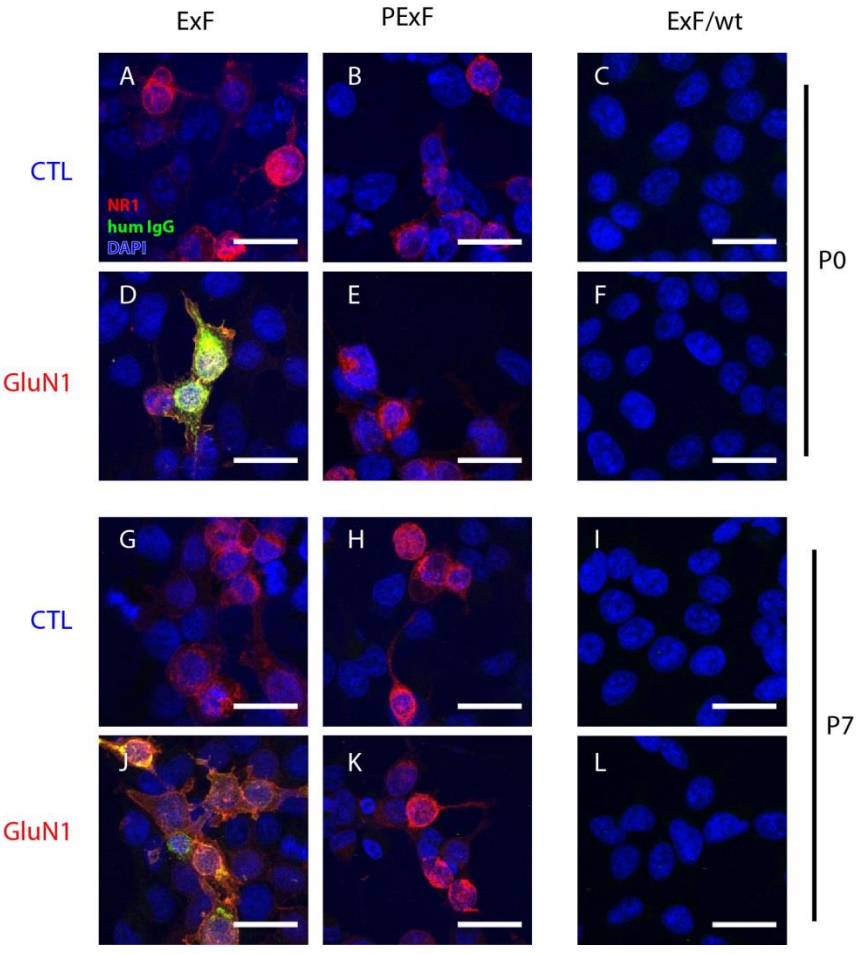

Figure 11: Staining of extracted human IgG from neonatal brain tissue on GluN1-transfected HEK cells. Brain IgG was extracted (ExF) from CTL (**A**-**C**, **G**-**I**) and GluN1 AB-treated neonates (**D**-**F**, **J**-**L**). Extracts from GluN1 AB-treated animals detect GluN1 on transfected HEK cells at P0 (**D**) and P7 (**J**), while no binding was detectable with ExF from CTL AB-treated animals (**A**, **G**). As negative controls, ExF of all animals did not bind to wildtype HEK cells (**C**, **F**, **I**, **L**). Also, none of the washing fractions (PExF) (**B**, **E**, **H**, **K**) bound to GluN-transfected HEK cells proving that extracted IgG is brain bound and not residual IgG.

3.4 NMDAR quantification

Synaptic localization of maternally transferred GluN1 AB stimulated the question, whether AB-antigen interaction leads to reduction of NMDAR, as proven by previous *in vitro* studies [18, 21]. Indeed, GluN1AB-treatment reduced NMDAR in synaptosomes (Figure 12, A), membrane fraction (Figure 12, B) and total cell fraction

(Figure 12, C) prepared from neonatal brains at day of birth with approximating levels at P7.

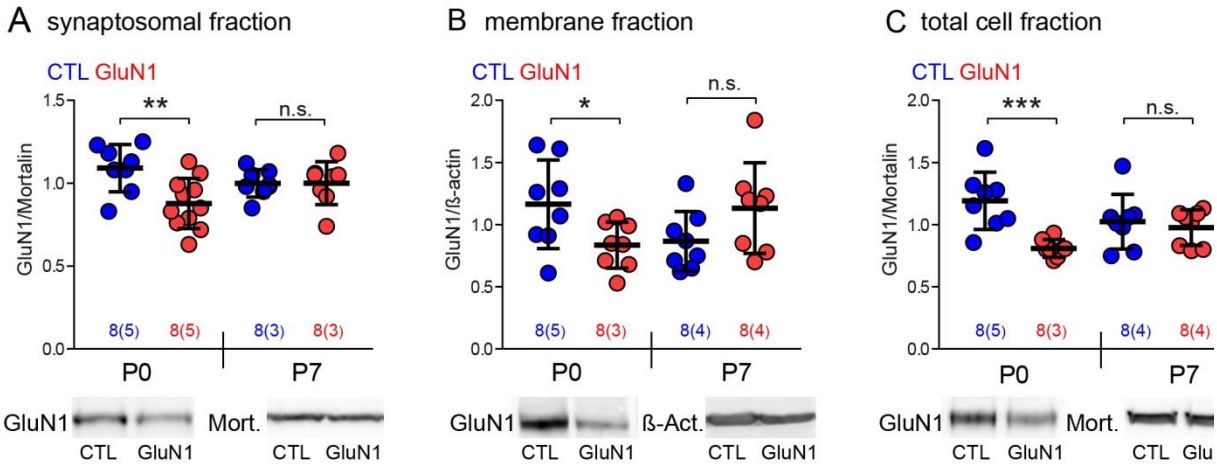

Figure 12: Quantification of NMDAR in neonatal brain tissue via Western Blot analysis.
Quantification of Western Blots with representative blots in lower row of synaptosomal (**A**), membrane (**B**) and total-cell fractions (**C**) prepared from neonatal brains depict GluN1 protein reduction in GluN1 AB-treated offspring at P0. Quantification showed significant GluN1 protein reduction in all three fractions (n=8 from 3-5 different litters; mean±SD, unpaired t-test; P0: p=0.0063 [A], p=0.0365 [B], p=0.0005 [C]) P7: p=0.9820 [A], p=0.1064 [B], p=0.6184 [C]).

As second approach, synaptic cluster quantification on neonatal brain sections was performed using another human, monoclonal GluN1 AB (see 2.2.10.1) directed against a different epitope (Figure 13, A, D) and postsynaptic marker Homer 1 (Figure 13, B, E). A ratio of double-positive punctae (GluN1$^+$/Homer1$^+$) to Homer1$^+$ single-positive punctae was calculated (Figure 13, C, F), reflecting synaptic GluN1 and therefore synaptic NMDAR. Quantification revealed drastically reduced levels of synaptic NMDAR clusters (49.2%) in GluN1 AB-treated offspring at P0 with less marked reduction at P7 (Figure 13, G).

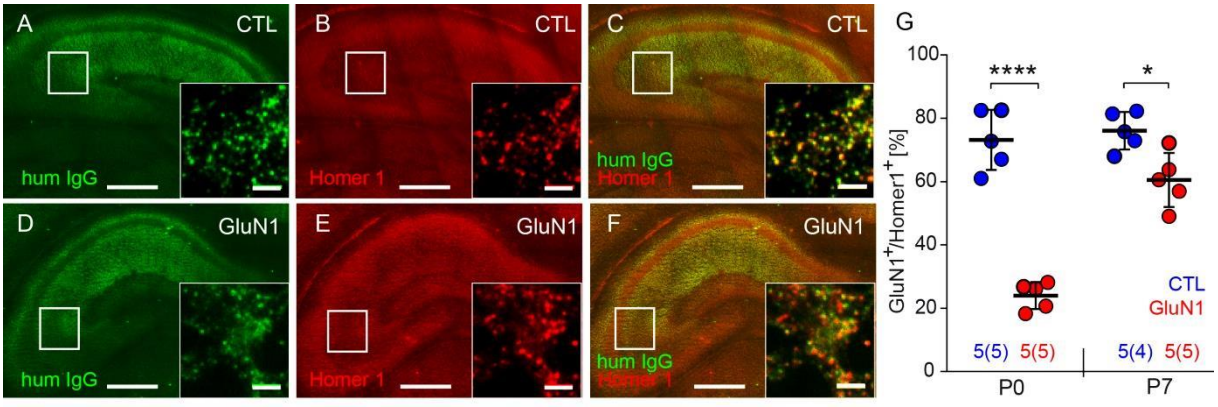

Figure 13: Quantification of synaptic NMDAR via immunofluorescence.
Quantification of co-localization of GluN1 positive punctae (**A**, **D**) to Homer 1 positive punctae (**B**, **E**; overlays in **C**, **F**) show marked decrease of GluN1^{+}/Homer1^{+}-clusters in GluN1 AB-treated animals compared to controls at P0 (**G**, n=5 from 5 different litters, mean±SD, unpaired t-test, p<0.0001), which was less pronounced at P7 (n=5 from 4-5 different litters, mean±SD, unpaired t-test, p=0.0102).

3.5 Electrophysiological recordings

It seemed highly plausible that this considerable reduction of GluN1 density would influence NMDAR signaling, whereupon electrophysiological properties of young neonatal brains were characterized. At day of birth and postnatal day seven, spontaneous excitatory postsynaptic currents (sEPSC) were recorded from acute slices by whole-cell-patch clamps from pyramidal neurons within the CA1 region of the hippocampus at -70mV. Analysis of recorded traces revealed a significant reduction in signal amplitude at day of birth that was diminished after seven days (Figure 14, C). The frequency of sEPSC was not altered by AB-treatment (Figure 14, D).

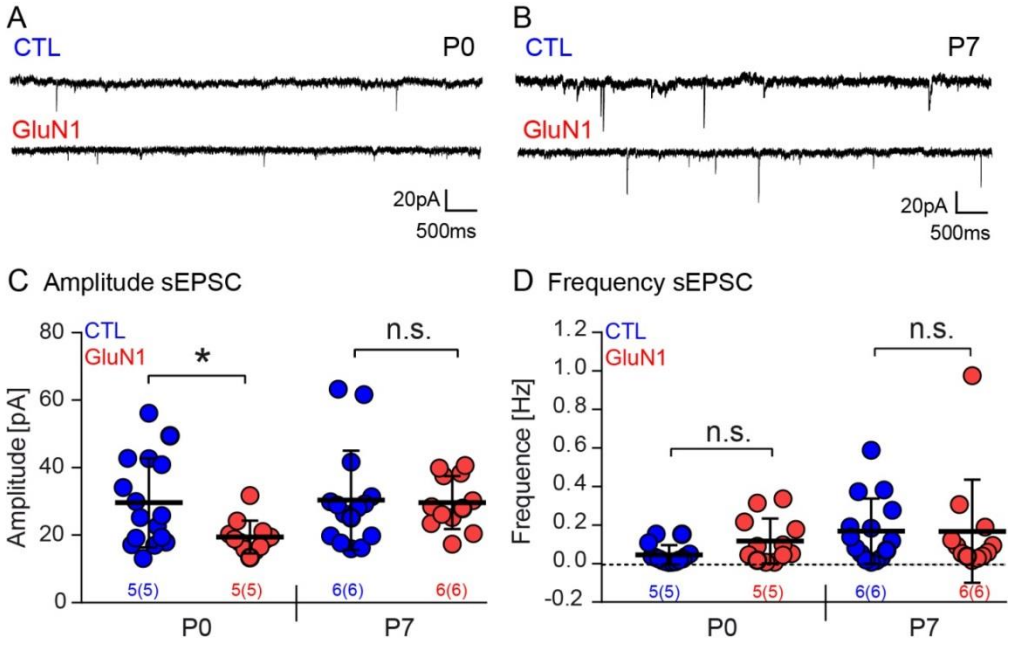

Figure 14: Electrophysiological properties of acute slices of neonatal brains.
Representative recordings of spontaneous excitatory postsynaptic currents (sEPSC) in neonatal brain slices at P0 (**A**) and P7 (**B**). Quantification revealed marked reduction of sEPSCs amplitudes at P0 (n=16 [CTL] and 12 [GluN1] cells from 5 neonates from 5 different litters, mean±SD, unpaired t-test, p=0.0176), which normalized until P7 (n=15 [CTL] and n=12 [GluN1] cells from 6 neonates from 6 different litters, P0: p=0.0882; P7: p=0.8825) (**C**). SEPSCs frequencies were not affected (**D**, mean±SD, unpaired t-test, P0: p=0.0688; P7: p=0.9939).

3.6 Physiological parameters

3.6.1 Mortality

A complete knock-out of the GluN1 subunit of the NMDAR in mice leads to early neonatal death within the first 24 hours [30]. As maternal GluN1 AB lead to NMDAR hypofunction in neonates, we hypothesized that treated offspring would also display reduced survival. In comparison to CTL AB-treated offspring, GluN1 AB-treated neonates displayed a 27.2% increased mortality within the first four days of neonatal life (Figure 15, A). This period seemed to be crucial, as animals that survived the first four days reached adulthood. Mortality was highly variable ranging from 0-100% within the first four days (Figure 15, B). The same phenomenon was observed with a higher concentration (Figure 15, B). The littersize *per se* did not differ between both groups, indicating that increased mortality is mediated by impairment of biological processes relevant for survival *ex utero* (Figure 15, C).

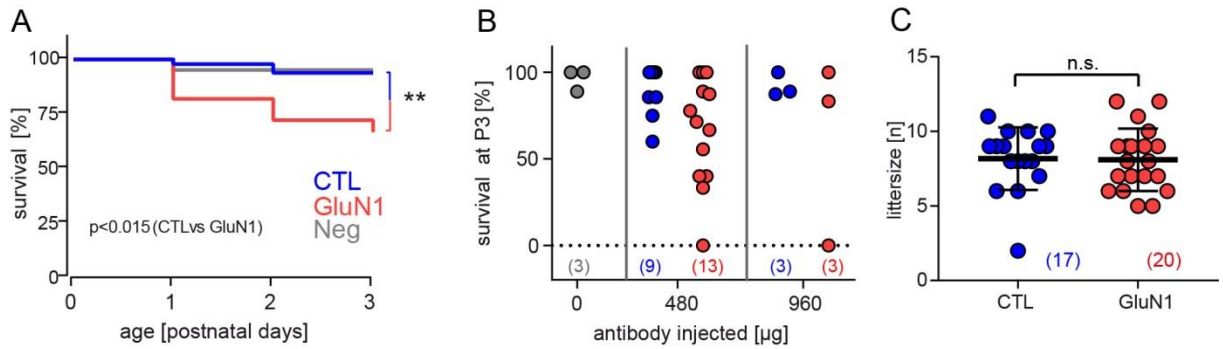

Figure 15: Survival rates and littersize of CTL and GluN1 AB-treated offspring.
Kaplan-Meier analysis of survival of young neonates showed significantly increased mortality in GluN1 AB-treated animals within the first four days (**A**, log-rank test, corrected with Bonferroni-correction for K=3, adjusted p=0.0015) compared to CTL animals). Survival rates of untreated, CTL and GluN1 AB-treated neonates at day P3 with different doses (**B**, untreated: n=3 litters; 480 µg: n=9 [CTL] and n=13 [GluN1]; 960 µg: n=3 [CTL] and n=3 [GluN1]). Litter size did not differ between both groups, excluding prepartum death of embryos (**C**, mean±SD n=17, mean= 8.2 [CTL], n=20, mean=8.1 [GluN1]).

Therefore, different aspects possibly influencing neonatal survival were investigated. As NMDAR are also essential components of circuitries responsible for basic functions like suckling behavior, milk intake was verified by surveying young neonates for milk spots. As animals were dying not immediately after birth within a rather long period of time, it seemed plausible that animals display reduced survival due to starving as a result of impaired suckling behavior. Offspring of both groups displayed milk spots within the first days, indicating normal milk uptake (Figure 16, A). As AB-treatment could potentially also affect the treated dam, maternal behavior was assessed by the

pups retrieval test. There was no significant difference between the groups neither in the latency to retrieve the first pup nor in the complete retrieval of all pups (Figure 15, B). Pups did also not show any sign of neglect or bitemarks. As NMDARE patients often suffer from respiratory dysfunction, it could be possible that exposure to GluN1 AB also lead to respiratory dysfunction in neonates that was

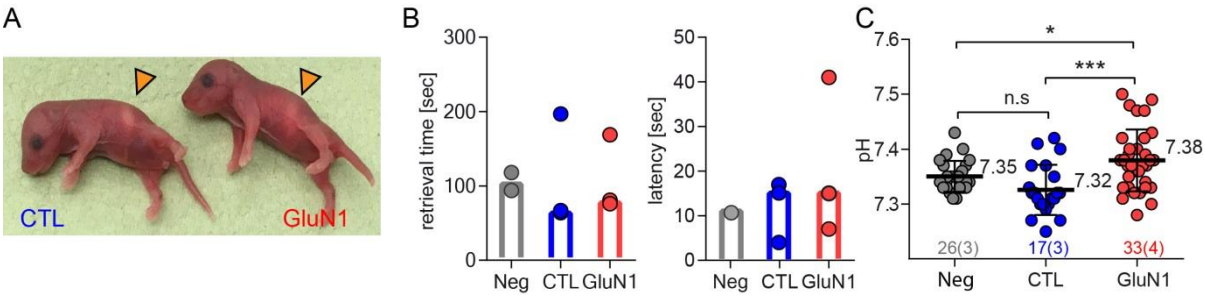

Figure 16: Suckling behavior, maternal behavior and neonatal blood pH.
Representative pictures of milk spots of newborn pups observed in both groups (**A**). Total retrieval time and latency to retrieve first pups is not significantly different between groups in the pups retrieval test (**B**, 2-3 dams/group, median with individual data points, Kruskal-Wallis test: retrieval p= 0.7571, latency p= 0.8286). Blood pH of untreated, CTL and GluN1 AB-treated neonates showed significantly elevated pH in the GluN1 group (**C**, untreated: n=26 from 3 litters, CTL AB: n=17 from 3 litters, GluN1 AB: n=33 from 4 litters, mean±SD, one-way ANOVA, post-hoc Tukey's multiple comparison test, untreated vs CTL AB: p=0.1685, untreated vs GluN1 AB: p=0.0488, CTL vs GluN1 AB: p=0.0002).

causal for increased mortality. Therefore, respiratory performance was assessed by analyzing blood pH at day of birth. Indeed, GluN1 AB-treated animals displayed a significantly increased blood pH in comparison to CTL AB-treated or untreated animals (Figure 16, C).

3.6.2 Bodyweight

As a robust parameter of normal/abnormal development, bodyweight of offspring was assessed during breast feeding period, post weaning, during adulthood and later in life (Figure 17). Observation detected significant reductions in bodyweight especially during breast-feeding period (Figure 17, A). After animals were weaned and sex-determined, differences in bodyweight were persistent in both females (Figure 17, B) and males (Figure 17, C) and diminished at adulthood, with both groups displaying similar bodyweight at 8 weeks and 10 months of age (Figure 17, B-C).

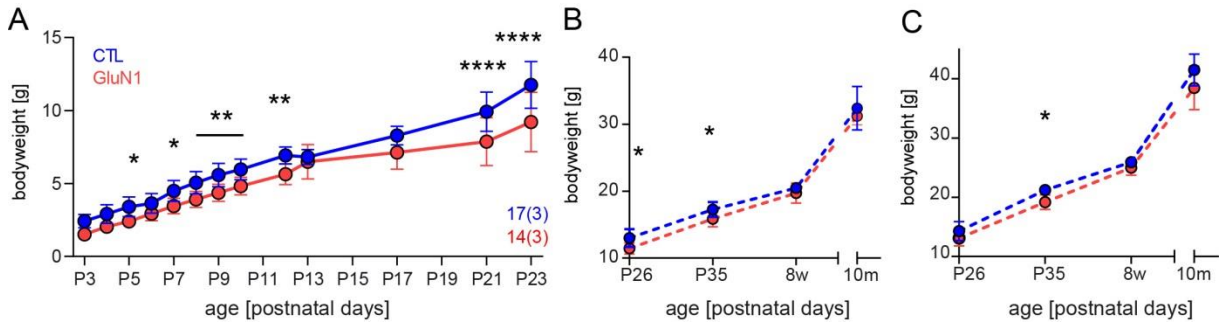

Figure 17: Development of bodyweight in neonates and adults.
Development of bodyweight of breastfed neonates (**A**), adult females (**B**) and adult males (**C**) after weaning (mean±SD, n=17 of 3 litters [CTL], n=14 of 3 litters [GluN1]; RM-ANOVA, Sidak's multiple comparison test).

3.6.3 Brain volumes

Analysis of brains from GluN1-knockout mice revealed that gross brain anatomy did not differ from wild type mice [30]. In order to investigate brain structure of mice exposed to maternal GluN1 AB, an MRI-based approach was used, and total brain and hippocampal volume was measured (Figure 18, A-C). Analysis of new-born pups did not show a significant difference in total brain volume (Figure 18, B) or hippocampal volume (Figure 18, C). In contrast to GluN1-knockout model, majority of GluN1 AB-treated offspring reaches adulthood and experience considerable brain growth. Therefore, also adult animals were measured via MRI-scans revealing significantly reduced total brain volumes in 10 month-old GluN1 AB-treated offspring (Figure 18, D).

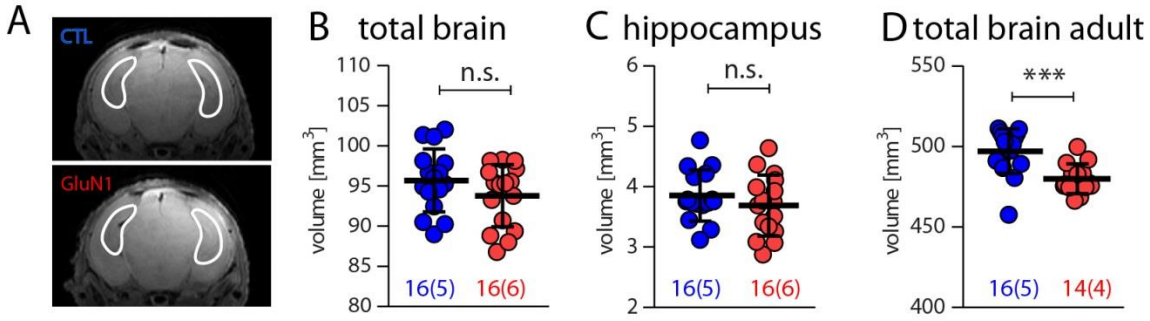

Figure 18: Brain volumes of young and old offspring determined by MRI measurements.
Representative MRI brain scans of CTL and GluN1 AB-treated neonates (P0) with highlighted hippocampal region (**A**). MRI-based quantification showed similar volumes in both groups for total brain volume (**B**, n=16, mean±SD, unpaired t-test, p=0.176) and hippocampus (**C**, n=16, mean±SD, unpaired t-test, p=0.3158). Total brain volumes of 10 month old mice showed highly significant differences in total brain volume (**D**, CTL n=16, GluN1 n= 14, mean±SD, unpaired t-test, p=0.0005).

Detailed analysis of pre-selected brain regions depicted highly significant changes especially in cerebellum, cerebral cortex, and brain stem (fference is treatment-specific (Table 5).

Table 4). In order to evaluate a potential sex-specific influence on brain volume, a two-way ANOVA of treatment vs sex was performed indicating that difference is treatment-specific (Table 5).

Table 4 Comparison of different brain regions of adult offspring (10 months)

	CTL			NR1						
Region [mm³]	**mean**	**SD**	**n**	**mean**	**SD**	**n**	**Diff.**	**p-value**	**hyp FDR**	**sign. level**
Cerebellum	48.60	1.49	16	44.61	1.23	14	-3.99	4.58E-08	y	****
Midbrain	24.25	0.96	16	22.92	0.50	14	-1.33	0.0612	n	
Brain stem	93.04	3.11	16	88.47	2.32	14	-4.58	4.94E-10	y	****
Pallidum	9.27	0.42	16	8.94	0.22	14	-0.33	0.6423	n	
Hypothalamus	13.52	0.85	16	12.90	0.60	14	-0.62	0.3805	n	
Cerebral cortex	190.90	5.36	16	187.26	3.68	14	-3.64	5.43E-07	y	****
Striatum	41.52	1.42	16	40.69	0.96	14	-0.84	0.2400	n	
Hippocamus	39.26	1.56	16	38.58	1.83	14	-0.68	0.3368	n	
Thalamus	21.71	0.71	16	21.38	1.02	14	-0.33	0.6399	n	
Amygdala	1.07	0.05	16	1.06	0.03	14	-0.01	0.9922	n	

SD= standard deviation; FDR=False discovery rate (Q=1%); hypFDR=significant discovery (1=yes, 0=no); sign. level= significance level

Table 5: Two-way ANOVA analysis of sex vs treatment interaction

	CTL			GluN1			
Analysis total brain vol. [mm3]	**mean**	**SD**	**n**	**mean**	**SD**	**n**	**Diff.**
male	496.52	7.92	6	479.05	9.92	9	-17.47
female	497.66	16.96	10	481.86	8.47	5	-15.80

Source of Variation	**% of total variation**	**P value**	**P value summary**	**Significant?**
Interaction	0.07743	0.8606	ns	No
sex	0.4363	0.6773	ns	No
treatment	30.86	0.0015	**	Yes

3.6.4 Activity

Similar to animal models of schizophrenia that are based on NMDAR hypofunction [35], offspring treated with GluN1-AB during fetal and early postnatal period display increased activity in the dark (active) phase during adulthood (week 12-14) when recorded over 14 days in their home cage (Figure 19 A-B).

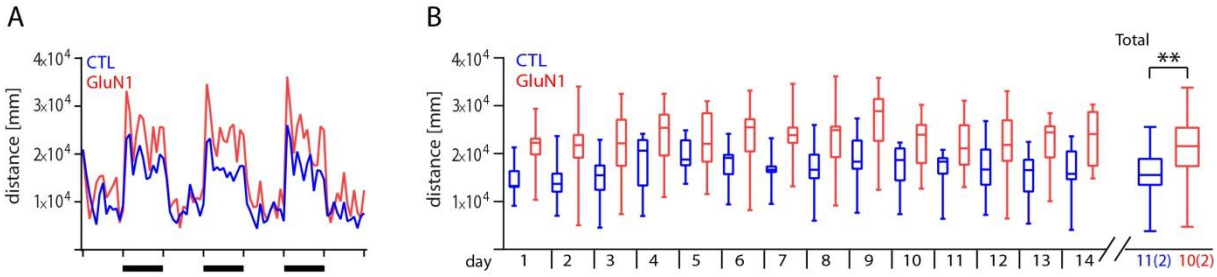

Figure 19: Activity recordings of treated offspring over 14 days.
Representative recordings of activity (mean of distance traveled) in home cages during three dark (black bars) and four light phases of adult offspring (**A**). In dark phases, home cage activity (boxplots of distance traveled) of GluN1 (n=10) compared to CTL AB-treated animals (n=11) was consistently higher during 14 days and in total (**B**, boxplots: median, 25-75 quartile, min-max; Wilcoxon-test of dark phase over all days, test score=179, p=0.0049).

3.7 Neonatal reflexes

Besides bodyweight measurement, assessment of establishment of reflexes is a robust marker for proper neonatal development. Usually, the age at which a certain milestone of neonatal development is achieved, reflects maturation process of neurodevelopment. Three typical tests have been chosen to evaluate progress in reflex establishment of CTL and GluN1 AB-treated offspring: verification of righting reflex (Figure 20, A), cliff avoidance (Figure 20, B) and negative geotaxis (Figure 20, C). Righting reflex is the pups' ability to put itself back on all feet, when placed on the back. Usually it is established between P2 and P10, with average at P5 [67]. Around P8 (P2-P12), mice develop the ability to detect a cliff and to turn away from it, without eyesight ("cliff avoidance"). When placed on an inclined plane, with head facing downwards, mice turn around and climb upwards the inclined plane, a reflex called negative geotaxis established around P3 and P15 (average P7). GluN1 AB-treated mice experience delays in all three reflexes, when compared to CTL AB-treated group (Figure 20). Interestingly, within in the first neonatal days, performance of both groups seems to be similar or even the same (Figure 20, A-C). But then, performance significantly drops in GluN1 AB-treated mice around postnatal day 5/6 till day 8/9.

Establishment of all reflexes is facilitated at same time as CTL AB-treated mice (P11) but progress is delayed.

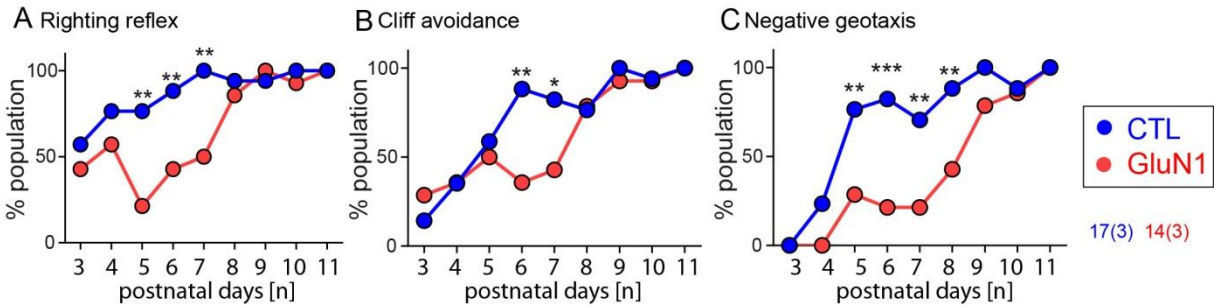

Figure 20: Development of neonatal reflexes.
Delayed development of the righting reflex (**A**), cliff avoidance (**B**) and negative geotaxis (**C**) in GluN1 AB-treated neonates compared to controls (3 litters, n=17 [CTL], n=14 [GluN1], points symbolize % of population showing the respective reflex, one-sided Fisher's exact test for each day. A: P5 p=0.0031, P6 p=0.010, P7 p=0.0013; B: P6 p=0.0034, P7 p=0.0275; C: P5 p=0.010, P6 p=0.001, P7 p=0.0082, P8 p=0.010).

3.8 Behavioral outcome

NMDAR hypofunction can affect many behavioral traits ranging from altered social behavior, schizophrenia-like behavior to deficits in learning and memory and many more [44]. For this study, well-established paradigms for distinct behavioral changes related to NMDAR hypofunction were used in order to characterize the behavioral profile of AB-treated animals.

3.8.1 Social behavior

Rats treated with NMDAR antagonist PCP [32] and mice expressing low levels of GluN1 [38] showed reduced social interaction. It seemed likely that offspring exposed to GluN1-AB may also display altered social behavior. However, analysis of social behavior in a 3-Chamber-Sociability test revealed no differences between both groups when investigating preference for an unknown (stranger) mouse compared to an object (Figure 21, A).

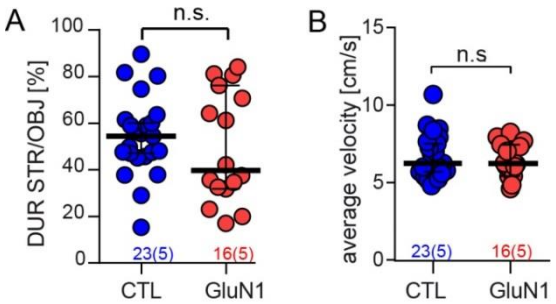

Figure 21: Social behavior in the 3-Chamber-Sociability test
No difference was observed in social preference in the 3-Chamber-Sociability test (**A**, DUR= duration, STR= stranger mouse, OBJ=object; n=23 [CTL], n=16 [GluN1] from 5 litters, median±95%CI, Mann-Whitney-U-test, p=0.4115). Animals of both groups showing similar velocity (**B**, median±95%CI, Mann-Whitney-U-test, p= 0.9494).

3.8.2 Learning and memory

As NMDAR are highly expressed in the hippocampal region, it was hypothesized that learning and memory function in GluN1-AB treated offspring might be impaired. For hypothesis evaluation, mice performed the Barnes Maze test where animals had to find the correct hole provided with a nest out of 20 holes on a platform. Ability of learning was assessed by the latency to find the correct hole over all 16 training trials (4 trials on 4 days) and statistically analyzed by calculating a ratio of first startle reaction minus last startle reaction divided by first startle reaction (Δ max-min/max). Both groups learned fast with highest progression within the first day of training (Figure 22, A) and equal efficiency (Figure 22, A') without velocity being affected (Figure 22, B). At day five (24h after last training day) and day 12 (seven days after last training day), mice were tested for memory recall, by assessment of latency for the correct zone (Figure 22, C) which did not differ between groups.

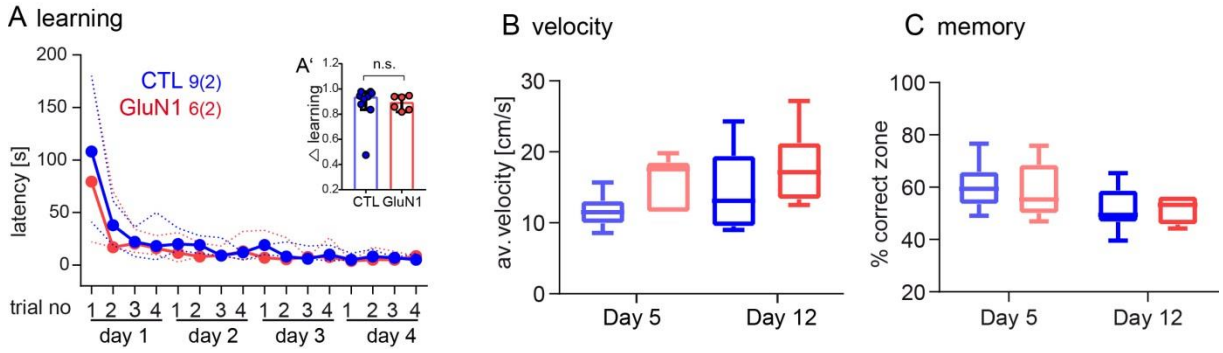

Figure 22: Learning and Memory in the Barnes Maze test
Animals of both groups showed rapid learning in Barnes Maze test (**A**, latency time to find correct hole of all four trials of all four training days, n=9 [CTL], n=6 [GluN1] from 2 litters, median±95%CI (dashed lines). Learning defined as ratio of difference of latency from first to last trial/latency of first trial was not significantly different (**A'**, Δ learning, median±95%CI, Mann-Whitney-U-test, p=0.4044). Between groups velocity was also not significantly different at day 5 or day 12 (**B**, 24 h after last training day or seven days respectively. Boxplots: median, 25-75 quartile, min-max, Kruskal-Wallis-test, p=0.0539). Memory recall was also not affected by AB-treatment (**C**, Boxplots: median, 25-75 quartile, min-max, Kruskal-Wallis-test, p=0.1322).

3.8.3 Sensorimotor gating functions

Exposure to a strong acoustic stimulus leads to startle reaction in humans, mice, rats, etc. When paired with milder pre-pulse milliseconds in advance to the strong acoustic stimulus, startle response is less pronounced. This phenomenon is called "Pre-pulse inhibition" (PPI) and reflects the filtering process also known as sensorimotor gating. Originally described in patients with schizophrenia, impairments in sensorimotor gating function have been described in multiple but not all psychiatric disorders [72]. An

acoustic startle response test to determine PPI can be easily applied in rodents. Nine-week-old offspring were exposed to several pre-pulse conditions to evaluate possible sensorimotor gating dysfunction (Figure 23). The general startle intensity did not vary between groups (Figure 23, A) and also the ability to habituate to the strong acoustic startle was not altered (Figure 23, B and B') together building the basis for an adequate interpretation of the results of PPI at different pre-pulse intensities. Statistical analysis revealed a significantly reduced PPI in GluN1-AB treated offspring at the mildest pre-pulse of 69 dB (Figure 23, C).

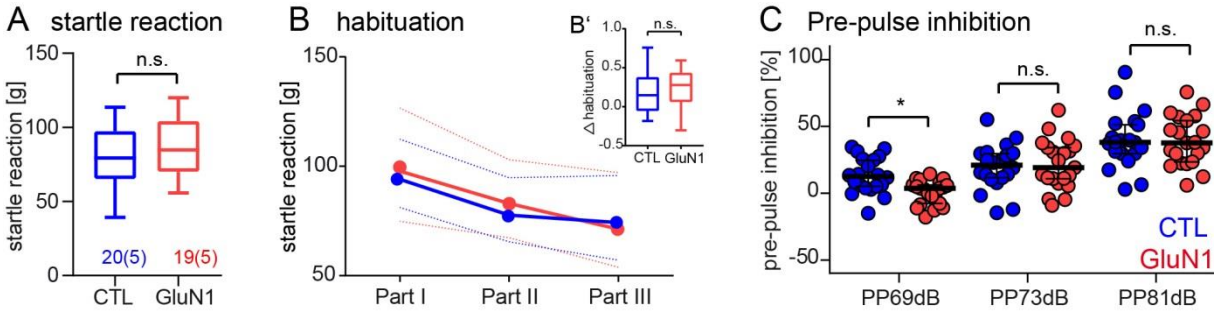

Figure 23: Evaluation of sensorimotor-gating function via Acoustic Startle Response test
Startle reaction intensity (median of all 120 dB stimuli) does not vary between groups (**A**, n=20 [CTL], n=21 [GluN1] from 5 litters, boxplots: median, 25-75 quartile, min-max; Mann-Whitney-U-test: p= 0.3532). Both groups habituate to acoustic stimuli (120 dB stimulus) as measured by reduction in startle reaction intensity over time (**B**, Part I: trial 1-5, Part II: trial 6-15, Part 3: trial 16-20). Analysis of difference between median startle reaction intensity of first to last part/first part revealed no significant difference in habituation (B', Δ habituation, median±95%CI Mann-Whitney-U-test, p=0.5170). Pre-pulse inhibition determined by startle reaction showed impaired sensorimotor gating in GluN1 AB-treated mice (**C**, median+95%CI, Kruskal-Wallis-test with Dunn's post-hoc test: Pp69dB p=0.0263, Pp73dB p=0.7964, Pp81dB p=0.9650).

3.8.4 Anxiety-like behavior

Eight-week-old offspring were tested for altered anxiety-like behavior in an Elevated Plus Maze test, where entries in open and closed arms reflect exploratory behavior and anxiety behavior. Analysis of 5 min exploration phase showed reduced anxiety-like behavior in GluN1-AB treated offspring, as indicated by increased duration and visits in open arms (Figure 24, A and B) which was not due to increased velocity Figure 24, C).

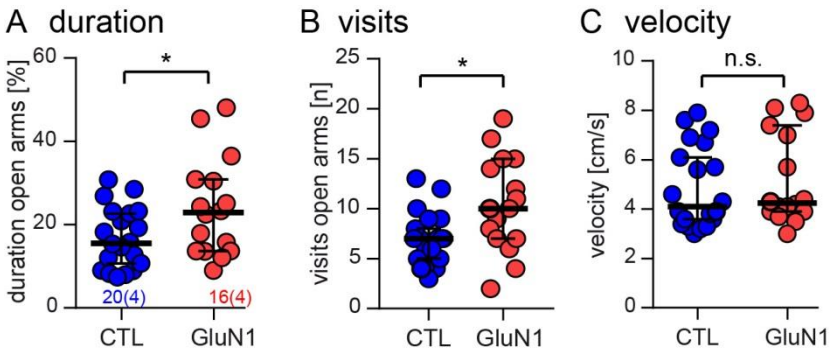

Figure 24: Anxiety behavior measured by the Elevated Plus Maze test
GluN1 animals displayed decreased anxiety behavior by increased duration in open arms (**A**, n=20 [CTL], n=16 [GluN1] from 4 litters, median+95%CI, Mann-Whitney-U-test, p=.0494) and increased entries into open arms of the elevated plus maze (**B**, p=0.0139). Velocity was not affected by AB treatment (**C**, p=0.3475).

3.8.5 Nest construction

Besides burrowing behavior, normal nest building is an indicator for general health and wellbeing in rodents. Assessing nest construction behavior implies to measure the amount of nestlet material used as well as the complexity of a nest, which has typically a dome-shaped structure build by shredded material. Mice with hippocampal lesion show deficits in nest complexity and use less nestlet material [70]. To verify if NMDAR reduction may also lead to impaired nest construction behavior, nests were weight and scored for two consecutive days (Figure 25). Nest construction appears to be normal in both groups as neither amounts of used nestlet material (Figure 25, A) nor nest complexity differed (Figure 25, B).

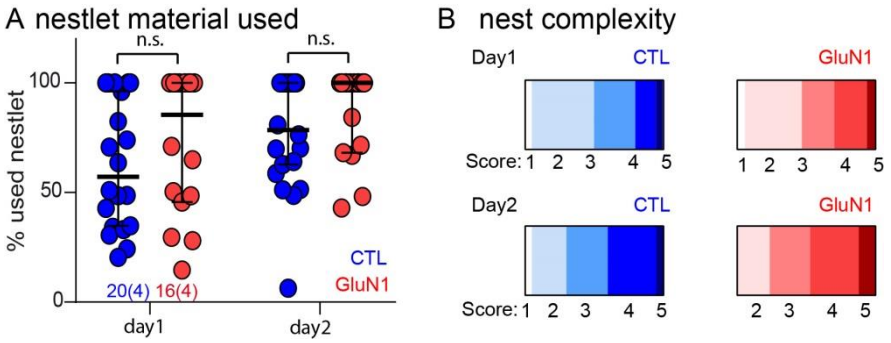

Figure 25: Nest construction behavior
Nest construction behavior assessed by weight of unused nestlet material (**A**, n=20 [CTL], n=16 [GluN1] from 4 litters, median+95%CI, Kruskal-Wallis-test, p=0.0718) and scored nest complexity (**B**) did not differ between groups.

3.8.6 Individual behavior in home cage

As a more ethoexperimental approach, individual behavior was recorded of each animal in a home cage. Intended to detect abnormalities in circadian cycles and repetitive behavior, animals were video recorded for 23 hours (10 -11 a.m., time of changing) and their distinct behaviors were analyzed (Figure 26). There were no significant differences in all behaviors analyzed.

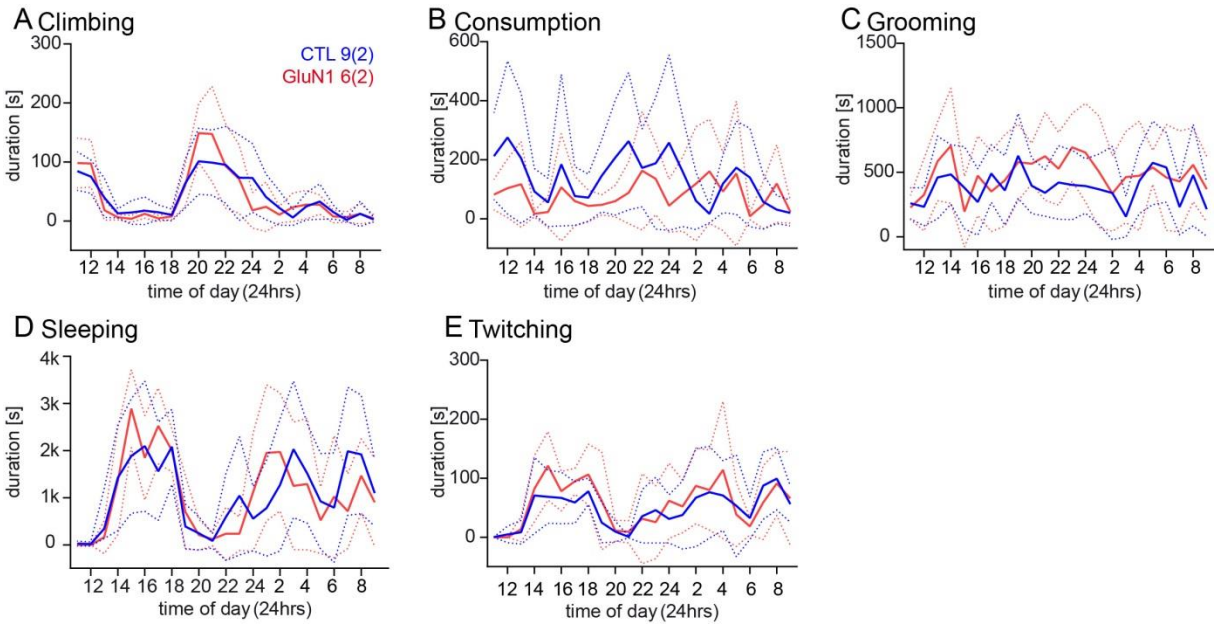

Figure 26: Distinct behavior in Home Cage Scan analysis
Distinct behavior was recorded with a Home Cage Scan system for each individual mouse and did not show significant differences in any recorded behavior, including climbing behavior (**A**, n=9 [CTL], n=6 [GluN1] [A-E], mean±SD [dotted lines], RMANOVA; between-subject-factor p=0.9957), consumption (eating + drinking) behavior (**B**, between-subject-factor p=0.1857), grooming behavior (**C**, between-subject-factor p=0.1700), sleeping behavior (**D**, p=0.9628) and twitching behavior (**E**, between-subject-factor p=0.3562).

3.8.7 Motoric abilities in Rotarod test

As MRI-analysis revealed significant reduction in total brain volume, cerebral cortex, brain stem and cerebellum, one-day Rotarod test (3 consecutive trials) were performed by ten-month-old animals in order to detect possible motoric dysfunction. GluN1 AB-treated offspring did not show differences in motor function as measured by latency to fall from rotating rod compared to CTL AB-treated animals (Figure 27).

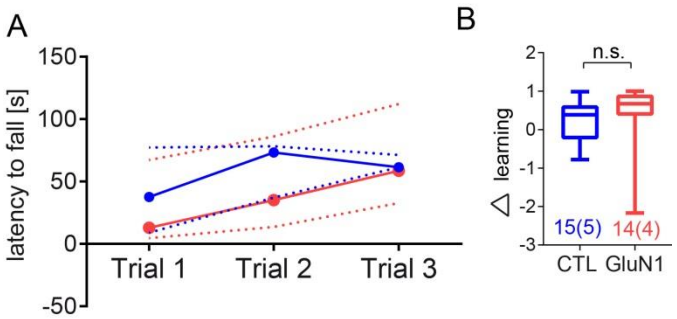

Figure 27: Assessment of motor function in Rotarod test

Both groups showed the same motoric abilities as measured by increasing latency to fall over three trials (**A**). Learning as calculated by a ratio of (lat_{Trial3} – lat_{Trial1})/ lat_{Trial3} did not differ between groups (**B**, Δ learning, median±95%CI Mann-Whitney-U-test, p= 0.1456).

4. Discussion

The here established model proved that maternally transferred GluN1 AB have neurotoxic potential as interaction with fetal and neonatal NMDAR led to profound changes in the offspring affecting neurodevelopment, survivability, physiology and behavior. In detail, GluN1 AB-treated young offspring displayed reduced NMDAR density accompanied by altered NMDAR signaling, increased mortality (+27%), reduced bodyweight, delays in neonatal reflex establishment, abnormal behavior and reduced brain volumes in adulthood.

Similar to humans, transfer of IgG in mice is facilitated by the neonatal Fc-receptor (FcRn) that actively transfers maternal IgG into fetal circulation in order to protect the newborn from infectious agents. In mice, the FcRn is located in the yolk sac and IgG is also transferred via breast milk [64, 73]. As in humans, the fetal and neonatal BBB is not fully developed [65] creating a critical window, where neuronal autoantibodies can interfere with establishment of essential circuitries. The observed enrichment in neonatal circulation and even more so within the brain pose a risk for pregnant women to transfer pathogenic amounts of GluN1 AB that may impair proper development in their children, even with low AB titers in the mothers.

Other murine models support the pathogenicity of maternally transferred autoantibodies. For example, active immunization against DNA of NR2B in a mouse model of systemic lupus erythemadosus (SLE) caused prenatal death of female mice, altered cortical development and provoked learning disabilities [56], providing an explanation for a higher incidence of learning disabilities in children of mothers with SLE. Injection of human sera from mothers with children suffering from ASD into pregnant dams resembled an autistic phenotype in murine offspring with developmental delays and increased anxiety-like behavior [58]. CASPR2 antibodies got into focus within the last years as they were suspected to be causal for some developmental abnormalities. Two studies could prove their pathogenicity: 1. Human IgG extracts from CASPR2-encephalitis patients disturbed proper cortical layer formation, increased microglial activity and altered social behavior in the offspring from treated dams [59]. 2. Application of a single monoclonal CASPR2 AB generated from a mother with an ASD child into pregnant mice mediated an ASD-like phenotype in their male offspring with impaired cortical development and behavioral abnormalities, especially social behavior [60].

NMDAR are involved in various steps and stages during fetal and neonatal brain development. A complete knockout of the GluN1 subunit stresses out the importance of the GluN1 subunit and the NMDAR in mammals *per se* as a complete knockout leads to early neonatal death in mice [30]. Interaction of GluN1 AB with NMDAR led to receptor internalization as it has already been shown *in vitro* [18] and *in vivo* [20], which was not mediated by complement activation [18]. Also in our model of maternal GluN1 AB transfer, AB interaction generated considerable reduction of NMDAR density verifying hypothesis 1 (see 1.8). By observing a decrease in all fractions (synaptosomal, membrane and total cell fraction), internalization of the receptor with subsequent degradation is more plausible than a drift of NMDAR out of the synaptic cleft, which would not lead to a reduction in membrane fraction and total cell fraction.

This internalization mediated a decrease in amplitude of spontaneous EPSCs in acute slices of newborn murine neonates as postulated in hypothesis 1 (see 1.8). These recordings were performed at -70 mV and therefore reflect AMPAR-mediated currents as NMDAR are voltage-dependent and are blocked by magnesia at resting membrane potential. Lagged recordings at +40 mV that reflect also NMDAR currents were performed but resulted in insufficient amount of successful recordings. In general, activity in newborn acute slices is minor, exacerbating investigation of electrophysiological properties and this was, to our knowledge, the first study using P0 pups. The results obtained suggest that AB-mediated NMDAR reduction leads to reduced AMPAR insertion and therefore to reduced amplitudes of AMPAR-mediated sEPSCs in newborn pups. At later stage (P7) AB-mediated effects on NMDAR density and signaling are diminished while AB levels in neonatal blood and brain are high in GluN1 AB-treated mice. This suggests a pivotal time frame for GluN1 AB during early neonatal life when expression of NMDAR is low [10, 11].

NMDAR are also involved in correct layer formation during development by facilitating migration of neuronal precursor cells [14]. Inhibition of NMDAR e.g. by interaction of GluN2B AB reduced cortical plate width in embryonic mice [56]. In humans, reduced brain volumes are observed in schizophrenic patients [74] and reversible frontotemporal atrophy is observed in some NMDARE-patients [75]. Contradictory to our hypothesis 5 (see 1.8), adult offspring of GluN1 AB-treated dams displayed strongly reduced volumes of total brain and especially cortex and cerebellum, pinpointing to long-lasting AB-mediated changes that were not gender-specific. Young

neonates did not display a significant difference in brain volume comparable to GluN1 knockout mice, which may indicate that differences manifest during activity dependent synapse formation and brain growth after birth. Further anatomic analysis is necessary to evaluate the role of a potential malformation of layers and a reduction of grey and/or white matter in general.

Exposure to maternal GluN1 AB affects survivability as expected by the observation of early neonatal death in GluN1 knockout mice [30]. As GluN1 AB lead to receptor hypofunction but not complete loss-of-function, usually not all pups were affected. On average 27% of GluN1 AB-treated animals did not survive the first 4 days but survival varied from 0% (no pups survived) to 100% (all pups survived). This variability suggests additional factors potentially relevant for mortality or AB distribution such as injection (e.g. accidental *in utero* application), anatomic/genetic variation of the dams or littersize (smaller littersize = higher individual AB concentration for each pup). As littersizes are not decreased in GluN1 AB-treated mice *per se*, mortality is due to impairment in vital functions essential for survival after birth. Potentially, maternal behavior of the dam could have been affected by GluN1 AB treatment and causal for early neonatal death. But offspring displayed neither signs of neglect nor bitemarks and dams showed normal caring behavior in the pup retrieval test. Also suckling behavior did not seem to be affected either as all pups displayed milk spots, an indicator for normal milk uptake. NMDAR are also involved in autonomic processes like respiration. Therefore, blood pH was analyzed to evaluate respiratory dysregulation as potential cause for early neonatal death, given that blood pH is also regulated by respiration status. Indeed, blood pH of GluN1 AB-treated neonates was significantly elevated in comparison to CTL AB- or untreated animals, indicating hyperventilation or metabolic changes. The findings parallel clinical observations, as NMDARE patients suffer from dysregulation of respiration as displayed by hypo- and hyperventilation [76]. Blood pH is a tightly regulated parameter where subtle changes affect other vital functions. The difference observed in GluN1 AB-treated offspring is highly significant but still in the range of a physiological pH. The observed effect might be time-dependent with potentially milder effects in early neonatal life that eventually escalate later on. Due to limited blood volume, other parameters evaluating the role of respiration status on altered blood pH (pCO_2, pO_2) could not be determined so that a metabolic malfunction cannot be excluded. These findings partially support and

disaccord hypothesis 2 (see 1.8), as animals do show reduced bodyweight and indication for respiratory malfunction but normal milk uptake.

Our murine model of GluN1 AB transfer resembles various models of neuropsychiatric disorders and developmental disorders. Similarities in reduced bodyweights are observed [58] and delays in establishment of neonatal reflexes [40, 56] which verify hypothesis 3 (see 1.8). Intriguingly, at first GluN1 AB-treated neonates show similar abilities compared to the CTL group within the first neonatal days but then the development is delayed between P5/6-P8/9. At postnatal day 9/10, reflexes improve and both groups establish the respective reflex simultaneously. Analysis of IgG concentration in neonatal blood and brain parenchyma revealed high levels in GluN1 AB-treated mice around P7 that potentially interfere with proper NMDAR function. In humans, delays in motor function are also observed in 51% of autistic children [77]. It indicates a time-dependent susceptibility to GluN1 AB-mediated disturbances on sensory and motor-circuit formation that are responsible for successful reflex establishment.

Also, the behavioral repertoire of GluN1 AB-treated offspring mirrors characteristic features of neuropsychiatric disorders. Hyperlocomotion is a hallmark of various neuropsychiatric disorders like schizophrenia, bipolar disorders and ADHD [78] . Murine offspring exposed to GluN1 AB also showed hyperactivity during adulthood in their home cage. Reduced anxiety is observed in ADHD patients and also GluN1 AB treated offspring displayed reduced anxiety as measured by increased duration and visits in the open arms of an Elevated Plus Maze. Treatment leads to mild reduction in PPI as observed by the acoustic startle response test. Disturbances in sensorimotor gating function and pre-conscious attention reflected by decreased PPI was initially thought to be specific for schizophrenia but has also been observed in other neuropsychiatric diseases like bipolar disorders and ADHD [72]. These changes accord with expected behavioral alternations in hypothesis 4 (see 1.8).

Altogether, behavioral changes are relatively subtle and do not resemble one distinct neuropsychiatric disorder but rather reflect aspects found in various diseases, making it to an interesting pathology potentially relevant to a broader group of diseases. The AB effect might even be stronger as only the surviving animals could be analyzed which might be less susceptible to GluN1 AB-mediated effects. Also, in humans GluN1 AB exposure might evoke subclinical changes during different stages of life that can

remain undiagnosed but still affecting quality of life. It is also highly plausible that a second hit (e.g. trauma, stress) could worsen the AB-mediated symptoms or lead to additional abnormalities.

First hints for the pathogenicity of maternal GluN1 AB also in humans come from clinical cases of NMDARE patients where pregnancy triggered onset or relapse of NMDARE. Evident neonatal developmental impairment was observed in approximately half of the babies of reported cases [79-82]. Unfortunately, the lack of follow-ups excludes adequate interpretation of long-lasting AB-mediated effects. In contrast to NMDARE patients with partial high AB-titer in serum and CSF, GluN1 AB subtype IgG are found in 1% of healthy blood donors, rendering GluN1 AB one of the most commonly diagnosed autoantibody [83]. The prevalence and relevance of low-titer NMDAR AB in pregnant women was recently investigated in mid-gestational serum samples of a Danish cohort including information about the developmental status of their respective children [84]. Significantly more NMDAR AB (29%) were found in mothers with schizophrenia spectrum disorders (SD) manifesting after birth of their first child, whose children were diagnosed with mental retardation and disorders of psychological development (MR/DPD) compared to SD mothers with children displaying normal behavior [84]. Notably, in other cohorts of healthy mothers with children suffering from MR/DPD or ASD, NMDAR AB prevalence was less prominent (<7%) and in the same range as in the control cohorts [84]. This further supports a paradigm of high prevalence of NMDAR AB also in pregnant women where a second hit may lead to manifestation of latent psychiatric abnormalities in their children.

Conclusion and outlook

Altogether, our model of maternal AB in mice clearly demonstrates the neurotoxic potential of GluN1 AB and their broad acute to long-lasting maleficial effects on the offspring. Due to AB-mediated mortality, effects may be even underestimated as surviving animals might be less sensitive to GluN1 AB. It also shows the far-reaching consequences of AB exposure as animals display not only impaired development in their early neonatal life but also behavioral and anatomical abnormalities during adulthood. As AB were considerably enriched in neonates, and dams did not show abnormal behavior, even complete asymptomatic pregnant women with low AB titer could be at risk to affect proper development of their children, clearly deserving further study.

This study stimulates the question whether an additional stressor would exaggerate negative AB-mediated effects (“second hit” hypothesis). Similar to investigations in transgenic mice expressing only 5% of physiological NMDAR levels [38], social isolation of AB-treated animals might be one experimental way to reveal the full spectrum of AB-mediated effects.

It also builds the basis for longitudinal studies in pregnant women with long follow-ups of their children in order to assess prevalence and a possible correlation of GluN1 AB and developmental disorders. If confirmed, this could have far-reaching implications by elaborating adequate therapy for pregnant women in order to potentially prevent psychiatric morbidities in children.

5. References

1. Johnson, J.W. and P. Ascher, *Glycine potentiates the NMDA response in cultured mouse brain neurons.* Nature, 1987. 325(6104): p. 529-31.
2. Mayer, M.L., G.L. Westbrook, and P.B. Guthrie, *Voltage-dependent block by Mg2+ of NMDA responses in spinal cord neurones.* Nature, 1984. 309(5965): p. 261-3.
3. MacDermott, A.B., M.L. Mayer, G.L. Westbrook, S.J. Smith, and J.L. Barker, *NMDA-receptor activation increases cytoplasmic calcium concentration in cultured spinal cord neurones.* Nature, 1986. 321(6069): p. 519-22.
4. Bliss, T.V. and G.L. Collingridge, *A synaptic model of memory: long-term potentiation in the hippocampus.* Nature, 1993. 361(6407): p. 31-9.
5. Rauner, C. and G. Kohr, *Triheteromeric NR1/NR2A/NR2B receptors constitute the major N-methyl-D-aspartate receptor population in adult hippocampal synapses.* J Biol Chem, 2011. 286(9): p. 7558-66.
6. Henson, M.A., A.C. Roberts, I. Perez-Otano, and B.D. Philpot, *Influence of the NR3A subunit on NMDA receptor functions.* Prog Neurobiol, 2010. 91(1): p. 23-37.
7. Paoletti, P., C. Bellone, and Q. Zhou, *NMDA receptor subunit diversity: impact on receptor properties, synaptic plasticity and disease.* Nat Rev Neurosci, 2013. 14(6): p. 383-400.
8. Watanabe, M., Y. Inoue, K. Sakimura, and M. Mishina, *Developmental changes in distribution of NMDA receptor channel subunit mRNAs.* Neuroreport, 1992. 3(12): p. 1138-40.
9. Feldman, D.E. and E.I. Knudsen, *Experience-dependent plasticity and the maturation of glutamatergic synapses.* Neuron, 1998. 20(6): p. 1067-71.
10. Laurie, D.J. and P.H. Seeburg, *Regional and developmental heterogeneity in splicing of the rat brain NMDAR1 mRNA.* J Neurosci, 1994. 14(5 Pt 2): p. 3180-94.
11. Monyer, H., N. Burnashev, D.J. Laurie, B. Sakmann, and P.H. Seeburg, *Developmental and regional expression in the rat brain and functional properties of four NMDA receptors.* Neuron, 1994. 12(3): p. 529-40.
12. Jantzie, L.L., D.M. Talos, M.C. Jackson, H.K. Park, D.A. Graham, M. Lechpammer, R.D. Folkerth, J.J. Volpe, and F.E. Jensen, *Developmental expression of N-methyl-D-aspartate (NMDA) receptor subunits in human white and gray matter: potential mechanism of increased vulnerability in the immature brain.* Cereb Cortex, 2015. 25(2): p. 482-95.
13. Bliss, T.V. and T. Lomo, *Long-lasting potentiation of synaptic transmission in the dentate area of the anaesthetized rabbit following stimulation of the perforant path.* J Physiol, 1973. 232(2): p. 331-56.
14. Byrne, J.H. and J.L. Roberts. *From molecules to networks : an introduction to cellular and molecular neuroscience*. 2004; xii, 583 p. ill. (some col.) 28 cm. + 1 CD-ROM (4 3/4 in.)]. Available from: Table of contents http://www.loc.gov/catdir/toc/els051/2003107472.html
15. Dalmau, J., E. Tuzun, H.Y. Wu, J. Masjuan, J.E. Rossi, A. Voloschin, J.M. Baehring, H. Shimazaki, R. Koide, D. King, W. Mason, L.H. Sansing, M.A. Dichter, M.R. Rosenfeld, and D.R. Lynch, *Paraneoplastic anti-N-methyl-D-aspartate receptor encephalitis associated with ovarian teratoma.* Ann Neurol, 2007. 61(1): p. 25-36.
16. Titulaer, M.J., L. McCracken, I. Gabilondo, T. Armangue, C. Glaser, T. Iizuka, L.S. Honig, S.M. Benseler, I. Kawachi, E. Martinez-Hernandez, E. Aguilar, N. Gresa-Arribas, N. Ryan-Florance, A. Torrents, A. Saiz, M.R. Rosenfeld, R. Balice-Gordon, F. Graus, and J. Dalmau, *Treatment and prognostic factors for long-term outcome in patients with anti-NMDA receptor encephalitis: an observational cohort study.* Lancet Neurol, 2013. 12(2): p. 157-65.
17. Gleichman, A.J., L.A. Spruce, J. Dalmau, S.H. Seeholzer, and D.R. Lynch, *Anti-NMDA receptor encephalitis antibody binding is dependent on amino acid identity of a small region within the GluN1 amino terminal domain.* J Neurosci, 2012. 32(32): p. 11082-94.

18. Hughes, E.G., X. Peng, A.J. Gleichman, M. Lai, L. Zhou, R. Tsou, T.D. Parsons, D.R. Lynch, J. Dalmau, and R.J. Balice-Gordon, *Cellular and synaptic mechanisms of anti-NMDA receptor encephalitis.* J Neurosci, 2010. 30(17): p. 5866-75.
19. Moscato, E.H., X. Peng, A. Jain, T.D. Parsons, J. Dalmau, and R.J. Balice-Gordon, *Acute mechanisms underlying antibody effects in anti-N-methyl-D-aspartate receptor encephalitis.* Ann Neurol, 2014. 76(1): p. 108-19.
20. Planaguma, J., F. Leypoldt, F. Mannara, J. Gutierrez-Cuesta, E. Martin-Garcia, E. Aguilar, M.J. Titulaer, M. Petit-Pedrol, A. Jain, R. Balice-Gordon, M. Lakadamyali, F. Graus, R. Maldonado, and J. Dalmau, *Human N-methyl D-aspartate receptor antibodies alter memory and behaviour in mice.* Brain, 2015. 138(Pt 1): p. 94-109.
21. Kreye, J., N.K. Wenke, M. Chayka, J. Leubner, R. Murugan, N. Maier, B. Jurek, L.T. Ly, D. Brandl, B.R. Rost, A. Stumpf, P. Schulz, H. Radbruch, A.E. Hauser, F. Pache, A. Meisel, L. Harms, F. Paul, U. Dirnagl, C. Garner, D. Schmitz, H. Wardemann, and H. Pruss, *Human cerebrospinal fluid monoclonal N-methyl-D-aspartate receptor autoantibodies are sufficient for encephalitis pathogenesis.* Brain, 2016. 139(Pt 10): p. 2641-2652.
22. Pruss, H., J. Leubner, N.K. Wenke, G.A. Czirjak, C.A. Szentiks, and A.D. Greenwood, *Anti-NMDA Receptor Encephalitis in the Polar Bear (Ursus maritimus) Knut.* Sci Rep, 2015. 5: p. 12805.
23. Pan, H., B. Oliveira, G. Saher, E. Dere, D. Tapken, M. Mitjans, J. Seidel, J. Wesolowski, D. Wakhloo, C. Klein-Schmidt, A. Ronnenberg, K. Schwabe, R. Trippe, K. Matz-Rensing, S. Berghoff, Y. Al-Krinawe, H. Martens, M. Begemann, W. Stocker, F.J. Kaup, R. Mischke, S. Boretius, K.A. Nave, J.K. Krauss, M. Hollmann, F. Luhder, and H. Ehrenreich, *Uncoupling the widespread occurrence of anti-NMDAR1 autoantibodies from neuropsychiatric disease in a novel autoimmune model.* Mol Psychiatry, 2018.
24. Steiner, J., M. Walter, W. Glanz, Z. Sarnyai, H.G. Bernstein, S. Vielhaber, A. Kastner, M. Skalej, W. Jordan, K. Schiltz, C. Klingbeil, K.P. Wandinger, B. Bogerts, and W. Stoecker, *Increased prevalence of diverse N-methyl-D-aspartate glutamate receptor antibodies in patients with an initial diagnosis of schizophrenia: specific relevance of IgG NR1a antibodies for distinction from N-methyl-D-aspartate glutamate receptor encephalitis.* JAMA Psychiatry, 2013. 70(3): p. 271-8.
25. Pruss, H., M. Holtje, N. Maier, A. Gomez, R. Buchert, L. Harms, G. Ahnert-Hilger, D. Schmitz, C. Terborg, U. Kopp, C. Klingbeil, C. Probst, S. Kohler, J.M. Schwab, W. Stoecker, J. Dalmau, and K.P. Wandinger, *IgA NMDA receptor antibodies are markers of synaptic immunity in slow cognitive impairment.* Neurology, 2012. 78(22): p. 1743-53.
26. Pruss, H., C. Finke, M. Holtje, J. Hofmann, C. Klingbeil, C. Probst, K. Borowski, G. Ahnert-Hilger, L. Harms, J.M. Schwab, C.J. Ploner, L. Komorowski, W. Stoecker, J. Dalmau, and K.P. Wandinger, *N-methyl-D-aspartate receptor antibodies in herpes simplex encephalitis.* Ann Neurol, 2012. 72(6): p. 902-11.
27. Castillo-Gomez, E., B. Oliveira, D. Tapken, S. Bertrand, C. Klein-Schmidt, H. Pan, P. Zafeiriou, J. Steiner, B. Jurek, R. Trippe, H. Pruss, W.H. Zimmermann, D. Bertrand, H. Ehrenreich, and M. Hollmann, *All naturally occurring autoantibodies against the NMDA receptor subunit NR1 have pathogenic potential irrespective of epitope and immunoglobulin class.* Mol Psychiatry, 2017. 22(12): p. 1776-1784.
28. Lemke, J.R., K. Geider, K.L. Helbig, H.O. Heyne, H. Schutz, J. Hentschel, C. Courage, C. Depienne, C. Nava, D. Heron, R.S. Moller, H. Hjalgrim, D. Lal, B.A. Neubauer, P. Nurnberg, H. Thiele, G. Kurlemann, G.L. Arnold, V. Bhambhani, D. Bartholdi, C.R. Pedurupillay, D. Misceo, E. Frengen, P. Stromme, D.J. Dlugos, E.S. Doherty, E.K. Bijlsma, C.A. Ruivenkamp, M.J. Hoffer, A. Goldstein, D.S. Rajan, V. Narayanan, K. Ramsey, N. Belnap, I. Schrauwen, R. Richholt, B.P. Koeleman, J. Sa, C. Mendonca, C.G. de Kovel, S. Weckhuysen, K. Hardies, P. De Jonghe, L. De Meirleir, M. Milh, C. Badens, M. Lebrun, T. Busa, C. Francannet, A. Piton, E. Riesch, S. Biskup, H. Vogt, T. Dorn, I. Helbig, J.L. Michaud, B. Laube, and S. Syrbe, *Delineating the GRIN1 phenotypic spectrum: A distinct genetic NMDA receptor encephalopathy.* Neurology, 2016. 86(23): p. 2171-8.

29. Lakhan, S.E., M. Caro, and N. Hadzimichalis, *NMDA Receptor Activity in Neuropsychiatric Disorders.* Front Psychiatry, 2013. 4: p. 52.
30. Forrest, D., M. Yuzaki, H.D. Soares, L. Ng, D.C. Luk, M. Sheng, C.L. Stewart, J.I. Morgan, J.A. Connor, and T. Curran, *Targeted disruption of NMDA receptor 1 gene abolishes NMDA response and results in neonatal death.* Neuron, 1994. 13(2): p. 325-38.
31. Li, Y., R.S. Erzurumlu, C. Chen, S. Jhaveri, and S. Tonegawa, *Whisker-related neuronal patterns fail to develop in the trigeminal brainstem nuclei of NMDAR1 knockout mice.* Cell, 1994. 76(3): p. 427-37.
32. Sams-Dodd, F., *Effect of novel antipsychotic drugs on phencyclidine-induced stereotyped behaviour and social isolation in the rat social interaction test.* Behav Pharmacol, 1997. 8(2-3): p. 196-215.
33. Adams, B. and B. Moghaddam, *Corticolimbic dopamine neurotransmission is temporally dissociated from the cognitive and locomotor effects of phencyclidine.* J Neurosci, 1998. 18(14): p. 5545-54.
34. Mansbach, R.S. and M.A. Geyer, *Effects of phencyclidine and phencyclidine biologs on sensorimotor gating in the rat.* Neuropsychopharmacology, 1989. 2(4): p. 299-308.
35. Mohn, A.R., R.R. Gainetdinov, M.G. Caron, and B.H. Koller, *Mice with reduced NMDA receptor expression display behaviors related to schizophrenia.* Cell, 1999. 98(4): p. 427-36.
36. Stefani, M.R. and B. Moghaddam, *Transient N-methyl-D-aspartate receptor blockade in early development causes lasting cognitive deficits relevant to schizophrenia.* Biol Psychiatry, 2005. 57(4): p. 433-6.
37. Halene, T.B., R.S. Ehrlichman, Y. Liang, E.P. Christian, G.J. Jonak, T.L. Gur, J.A. Blendy, H.C. Dow, E.S. Brodkin, F. Schneider, R.C. Gur, and S.J. Siegel, *Assessment of NMDA receptor NR1 subunit hypofunction in mice as a model for schizophrenia.* Genes Brain Behav, 2009. 8(7): p. 661-75.
38. Gandal, M.J., R.L. Anderson, E.N. Billingslea, G.C. Carlson, T.P. Roberts, and S.J. Siegel, *Mice with reduced NMDA receptor expression: more consistent with autism than schizophrenia?* Genes Brain Behav, 2012. 11(6): p. 740-50.
39. Won, H., H.R. Lee, H.Y. Gee, W. Mah, J.I. Kim, J. Lee, S. Ha, C. Chung, E.S. Jung, Y.S. Cho, S.G. Park, J.S. Lee, K. Lee, D. Kim, Y.C. Bae, B.K. Kaang, M.G. Lee, and E. Kim, *Autistic-like social behaviour in Shank2-mutant mice improved by restoring NMDA receptor function.* Nature, 2012. 486(7402): p. 261-5.
40. Single, F.N., A. Rozov, N. Burnashev, F. Zimmermann, D.F. Hanley, D. Forrest, T. Curran, V. Jensen, O. Hvalby, R. Sprengel, and P.H. Seeburg, *Dysfunctions in mice by NMDA receptor point mutations NR1(N598Q) and NR1(N598R).* J Neurosci, 2000. 20(7): p. 2558-66.
41. Reiprich, P., W. Kilb, and H.J. Luhmann, *Neonatal NMDA receptor blockade disturbs neuronal migration in rat somatosensory cortex in vivo.* Cereb Cortex, 2005. 15(3): p. 349-58.
42. Komuro, H. and P. Rakic, *Modulation of neuronal migration by NMDA receptors.* Science, 1993. 260(5104): p. 95-7.
43. Messersmith, E.K., M.B. Feller, H. Zhang, and C.J. Shatz, *Migration of neocortical neurons in the absence of functional NMDA receptors.* Mol Cell Neurosci, 1997. 9(5-6): p. 347-57.
44. Ewald, R.C. and H.T. Cline, *NMDA Receptors and Brain Development*, in *Biology of the NMDA Receptor*, A.M. Van Dongen, Editor. 2009: Boca Raton (FL).
45. Simon, D.K., G.T. Prusky, D.D. O'Leary, and M. Constantine-Paton, *N-methyl-D-aspartate receptor antagonists disrupt the formation of a mammalian neural map.* Proc Natl Acad Sci U S A, 1992. 89(22): p. 10593-7.
46. Brenneman, D.E., I.D. Forsythe, T. Nicol, and P.G. Nelson, *N-methyl-D-aspartate receptors influence neuronal survival in developing spinal cord cultures.* Brain Res Dev Brain Res, 1990. 51(1): p. 63-8.
47. Luo, T., W.H. Wu, and B.S. Chen, *NMDA receptor signaling: death or survival?* Front Biol (Beijing), 2011. 6(6): p. 468-476.

48. Ben-Ari, Y., R. Khazipov, X. Leinekugel, O. Caillard, and J.L. Gaiarsa, *GABAA, NMDA and AMPA receptors: a developmentally regulated 'menage a trois'.* Trends Neurosci, 1997. 20(11): p. 523-9.
49. Leinekugel, X., I. Khalilov, H. McLean, O. Caillard, J.L. Gaiarsa, Y. Ben-Ari, and R. Khazipov, *GABA is the principal fast-acting excitatory transmitter in the neonatal brain.* Adv Neurol, 1999. 79: p. 189-201.
50. Kutsuwada, T., K. Sakimura, T. Manabe, C. Takayama, N. Katakura, E. Kushiya, R. Natsume, M. Watanabe, Y. Inoue, T. Yagi, S. Aizawa, M. Arakawa, T. Takahashi, Y. Nakamura, H. Mori, and M. Mishina, *Impairment of suckling response, trigeminal neuronal pattern formation, and hippocampal LTD in NMDA receptor epsilon 2 subunit mutant mice.* Neuron, 1996. 16(2): p. 333-44.
51. Kubo, T. and M. Kihara, *Evidence of N-methyl-D-aspartate receptor-mediated modulation of the aortic baroreceptor reflex in the rat nucleus tractus solitarii.* Neurosci Lett, 1988. 87(1-2): p. 69-74.
52. Foutz, A.S., J. Champagnat, and M. Denavit-Saubie, *Involvement of N-methyl-D-aspartate (NMDA) receptors in respiratory rhythmogenesis.* Brain Res, 1989. 500(1-2): p. 199-208.
53. Bozic, M. and J.M. Valdivielso, *The potential of targeting NMDA receptors outside the CNS.* Expert Opin Ther Targets, 2015. 19(3): p. 399-413.
54. Qi, Q., F. Chen, W. Zhang, P. Wang, Y. Li, and X. Zuo, *Colonic N-methyl-d-aspartate receptor contributes to visceral hypersensitivity in irritable bowel syndrome.* J Gastroenterol Hepatol, 2017. 32(4): p. 828-836.
55. Warren, R.P., P. Cole, J.D. Odell, C.B. Pingree, W.L. Warren, E. White, J. Yonk, and V.K. Singh, *Detection of maternal antibodies in infantile autism.* J Am Acad Child Adolesc Psychiatry, 1990. 29(6): p. 873-7.
56. Lee, J.Y., P.T. Huerta, J. Zhang, C. Kowal, E. Bertini, B.T. Volpe, and B. Diamond, *Neurotoxic autoantibodies mediate congenital cortical impairment of offspring in maternal lupus.* Nat Med, 2009. 15(1): p. 91-6.
57. Singer, H.S., C. Morris, C. Gause, M. Pollard, A.W. Zimmerman, and M. Pletnikov, *Prenatal exposure to antibodies from mothers of children with autism produces neurobehavioral alterations: A pregnant dam mouse model.* J Neuroimmunol, 2009. 211(1-2): p. 39-48.
58. Braunschweig, D., M.S. Golub, C.M. Koenig, L. Qi, I.N. Pessah, J. Van de Water, and R.F. Berman, *Maternal autism-associated IgG antibodies delay development and produce anxiety in a mouse gestational transfer model.* J Neuroimmunol, 2012. 252(1-2): p. 56-65.
59. Coutinho, E., D.A. Menassa, L. Jacobson, S.J. West, J. Domingos, T.C. Moloney, B. Lang, P.J. Harrison, D.L.H. Bennett, D. Bannerman, and A. Vincent, *Persistent microglial activation and synaptic loss with behavioral abnormalities in mouse offspring exposed to CASPR2-antibodies in utero.* Acta Neuropathol, 2017. 134(4): p. 567-583.
60. Brimberg, L., S. Mader, V. Jeganathan, R. Berlin, T.R. Coleman, P.K. Gregersen, P.T. Huerta, B.T. Volpe, and B. Diamond, *Caspr2-reactive antibody cloned from a mother of an ASD child mediates an ASD-like phenotype in mice.* Mol Psychiatry, 2016. 21(12): p. 1663-1671.
61. Dalton, P., R. Deacon, A. Blamire, M. Pike, I. McKinlay, J. Stein, P. Styles, and A. Vincent, *Maternal neuronal antibodies associated with autism and a language disorder.* Ann Neurol, 2003. 53(4): p. 533-7.
62. Pentsuk, N. and J.W. van der Laan, *An interspecies comparison of placental antibody transfer: new insights into developmental toxicity testing of monoclonal antibodies.* Birth Defects Res B Dev Reprod Toxicol, 2009. 86(4): p. 328-44.
63. Palmeira, P., C. Quinello, A.L. Silveira-Lessa, C.A. Zago, and M. Carneiro-Sampaio, *IgG placental transfer in healthy and pathological pregnancies.* Clin Dev Immunol, 2012. 2012: p. 985646.
64. Van de Perre, P., *Transfer of antibody via mother's milk.* Vaccine, 2003. 21(24): p. 3374-6.

65. Braniste, V., M. Al-Asmakh, C. Kowal, F. Anuar, A. Abbaspour, M. Toth, A. Korecka, N. Bakocevic, L.G. Ng, P. Kundu, B. Gulyas, C. Halldin, K. Hultenby, H. Nilsson, H. Hebert, B.T. Volpe, B. Diamond, and S. Pettersson, *The gut microbiota influences blood-brain barrier permeability in mice.* Sci Transl Med, 2014. 6(263): p. 263ra158.
66. Koch, S., S. Mueller, M. Foddis, T. Bienert, D. von Elverfeldt, F. Knab, T.D. Farr, R. Bernard, M. Dopatka, A. Rex, U. Dirnagl, C. Harms, and P. Boehm-Sturm, *Atlas registration for edema-corrected MRI lesion volume in mouse stroke models.* J Cereb Blood Flow Metab, 2017: p. 271678X17726635.
67. Heyser, C.J., *Assessment of developmental milestones in rodents.* Curr Protoc Neurosci, 2004. Chapter 8: p. Unit 8 18.
68. Rogers, D.C., J. Peters, J.E. Martin, S. Ball, S.J. Nicholson, A.S. Witherden, M. Hafezparast, J. Latcham, T.L. Robinson, C.A. Quilter, and E.M. Fisher, *SHIRPA, a protocol for behavioral assessment: validation for longitudinal study of neurological dysfunction in mice.* Neurosci Lett, 2001. 306(1-2): p. 89-92.
69. Lipina, T., V. Labrie, I. Weiner, and J. Roder, *Modulators of the glycine site on NMDA receptors, D-serine and ALX 5407, display similar beneficial effects to clozapine in mouse models of schizophrenia.* Psychopharmacology (Berl), 2005. 179(1): p. 54-67.
70. Deacon, R., *Assessing burrowing, nest construction, and hoarding in mice.* J Vis Exp, 2012(59): p. e2607.
71. Wardemann, H., S. Yurasov, A. Schaefer, J.W. Young, E. Meffre, and M.C. Nussenzweig, *Predominant autoantibody production by early human B cell precursors.* Science, 2003. 301(5638): p. 1374-7.
72. Levin, R., M.B. Calzavara, C.M. Santos, W.A. Medrano, S.T. Niigaki, and V.C. Abilio, *Spontaneously Hypertensive Rats (SHR) present deficits in prepulse inhibition of startle specifically reverted by clozapine.* Prog Neuropsychopharmacol Biol Psychiatry, 2011. 35(7): p. 1748-52.
73. Kim, J., S. Mohanty, L.P. Ganesan, K. Hua, D. Jarjoura, W.L. Hayton, J.M. Robinson, and C.L. Anderson, *FcRn in the yolk sac endoderm of mouse is required for IgG transport to fetus.* J Immunol, 2009. 182(5): p. 2583-9.
74. Balu, D.T., *The NMDA Receptor and Schizophrenia: From Pathophysiology to Treatment.* Adv Pharmacol, 2016. 76: p. 351-82.
75. Iizuka, T., S. Yoshii, S. Kan, J. Hamada, J. Dalmau, F. Sakai, and H. Mochizuki, *Reversible brain atrophy in anti-NMDA receptor encephalitis: a long-term observational study.* J Neurol, 2010. 257(10): p. 1686-91.
76. Vural, A., E.M. Arsava, N. Dericioglu, and M.A. Topcuoglu, *Central neurogenic hyperventilation in anti-NMDA receptor encephalitis.* Intern Med, 2012. 51(19): p. 2789-92.
77. Ming, X., M. Brimacombe, and G.C. Wagner, *Prevalence of motor impairment in autism spectrum disorders.* Brain Dev, 2007. 29(9): p. 565-70.
78. Powell, C.M. and T. Miyakawa, *Schizophrenia-relevant behavioral testing in rodent models: a uniquely human disorder?* Biol Psychiatry, 2006. 59(12): p. 1198-207.
79. Kumar, M.A., A. Jain, V.E. Dechant, T. Saito, T. Rafael, H. Aizawa, K.C. Dysart, T. Katayama, Y. Ito, N. Araki, T. Abe, R. Balice-Gordon, and J. Dalmau, *Anti-N-methyl-D-aspartate receptor encephalitis during pregnancy.* Arch Neurol, 2010. 67(7): p. 884-7.
80. Hilderink, M., M.J. Titulaer, M.W. Schreurs, K. Keizer, and J.E. Bunt, *Transient anti-NMDAR encephalitis in a newborn infant due to transplacental transmission.* Neurol Neuroimmunol Neuroinflamm, 2015. 2(4): p. e126.
81. Jagota, P., A. Vincent, and R. Bhidayasiri, *Transplacental transfer of NMDA receptor antibodies in an infant with cortical dysplasia.* Neurology, 2014. 82(18): p. 1662-3.
82. Mathis, S., J.C. Pin, F. Pierre, J. Ciron, A. Iljicsov, M. Lamy, and J.P. Neau, *Anti-NMDA Receptor Encephalitis During Pregnancy: A Case Report.* Medicine (Baltimore), 2015. 94(26): p. e1034.
83. Dahm, L., C. Ott, J. Steiner, B. Stepniak, B. Teegen, S. Saschenbrecker, C. Hammer, K. Borowski, M. Begemann, S. Lemke, K. Rentzsch, C. Probst, H. Martens, J. Wienands, G. Spalletta, K. Weissenborn, W. Stocker, and H. Ehrenreich,

Seroprevalence of autoantibodies against brain antigens in health and disease. Ann Neurol, 2014. 76(1): p. 82-94.
84. Coutinho, E., L. Jacobson, M.G. Pedersen, M.E. Benros, B. Norgaard-Pedersen, P.B. Mortensen, P.J. Harrison, and A. Vincent, *CASPR2 autoantibodies are raised during pregnancy in mothers of children with mental retardation and disorders of psychological development but not autism.* J Neurol Neurosurg Psychiatry, 2017. 88(9): p. 718-721.

Eidesstattliche Versicherung

„Ich, Betty Jurek, versichere an Eides statt durch meine eigenhändige Unterschrift, dass ich die vorgelegte Dissertation mit dem Thema: „Effects of human anti-GluN1 antibodies on the offspring in a murine model of maternal antibody transfer“ selbstständig und ohne nicht offengelegte Hilfe Dritter verfasst und keine anderen als die angegebenen Quellen und Hilfsmittel genutzt habe.

Alle Stellen, die wörtlich oder dem Sinne nach auf Publikationen oder Vorträgen anderer Autoren beruhen, sind als solche in korrekter Zitierung (siehe „Uniform Requirements for Manuscripts (URM)“ des ICMJE -www.icmje.org) kenntlich gemacht. Die Abschnitte zu Methodik (insbesondere praktische Arbeiten, Laborbestimmungen, statistische Aufarbeitung) und Resultaten (insbesondere Abbildungen, Graphiken und Tabellen) entsprechen den URM (s.o) und werden von mir verantwortet.

Meine Anteile an etwaigen Publikationen zu dieser Dissertation entsprechen denen, die in der untenstehenden gemeinsamen Erklärung mit dem/der Betreuer/in, angegeben sind. Sämtliche Publikationen, die aus dieser Dissertation hervorgegangen sind und bei denen ich Autor bin, entsprechen den URM (s.o) und werden von mir verantwortet.

Die Bedeutung dieser eidesstattlichen Versicherung und die strafrechtlichen Folgen einer unwahren eidesstattlichen Versicherung (§156,161 des Strafgesetzbuches) sind mir bekannt und bewusst.“

Ort, Datum

Unterschrift

Lebenslauf

Mein Lebenslauf wird aus datenschutzrechtlichen Gründen in der elektronischen Version meiner Arbeit nicht veröffentlicht.

Publikationsliste (chronologisch)

1. Meyerson BJ, **Jurek B**, Roman E, *A Rank-Order Procedure Applied to an Ethoexperimental Behavior Model—The Multivariate Concentric SquareField™(MCSF) Test*, Journal of Behavioral and Brain Science, 2013, Vol. 3, no 4, p. 350-36
2. Jolivel V, Bicker F, Binamé F, Ploen R, Keller S, Gollan R, **Jurek B**, Birkenstock J, Poisa-Beiro L, Bruttger J, Opitz V, Thal SC, Waisman A, Bäuerle T, Schäfer MK, Zipp F, Schmidt MH, *Perivascular microglia promote blood vessel disintegration in the ischemic penumbra*., Acta Neuropathol, 2015 Feb, 129(2):279-95
3. Volz MS, Finke C, Harms L, **Jurek B**, Paul F, Flöel A, Prüss H, *Altered paired associative stimulation-induced plasticity in NMDAR encephalitis*, Ann Clin Transl Neurol, 2016 Jan 16;3(2):101-13
4. Kreye J, Wenke NK, Chayka M, Leubner J, Murugan R, Maier N, **Jurek B**, Ly LT, Brandl D, Rost BR, Stumpf A, Schulz P, Radbruch H, Hauser AE, Pache F, Meisel A, Harms L, Paul F, Dirnagl U, Garner C, Schmitz D, Wardemann H, Prüss H, *Human cerebrospinal fluid monoclonal N-methyl-D-aspartate receptor autoantibodies are sufficient for encephalitis pathogenesis*, Brain, 2016 Oct;139(Pt 10):2641-2652.
5. Castillo-Gómez E, Oliveira B, Tapken D, Bertrand S, Klein-Schmidt C, Pan H, Zafeiriou P, Steiner J, **Jurek B**, Trippe R, Prüss H, Zimmermann WH, Bertrand D, Ehrenreich H, Hollmann M, *All naturally occurring autoantibodies against the NMDA receptor subunit NR1 have pathogenic potential irrespective of epitope and immunoglobulin class*, Mol Psychiatry, 2017 Dec;22(12):1776-1784

Danksagung

Diese Arbeit wurde mir durch die Unterstützung vieler Menschen auf unterschiedlichsten Weisen ermöglicht, denen ich meinen größten Dank aussprechen möchte.

Meine tiefste Dankbarkeit gilt meinem Mann Dietmar, der mich zu diesem Abenteuer ermutigt, tagtäglich unterstützt und immer wieder aufs Neue motiviert hat.

Großen Dank möchte ich meinem Doktorvater Harald Prüß aussprechen, der mir von Anfang an großes Vertrauen schenkte und mir mit seiner offenen Art ermöglichte, mich wissenschaftlich und auch persönlich weiterzuentwickeln.

Besonderer Dank gilt allen, die diese Arbeit durch aktive Mitarbeit unterstützen:

- Mariya Chayka, Durchführung von Immunisierungen, Pflege der Tiere, Asservierung von Proben, Blut-pH-Bestimmungen, IgG-Extraktionen, GluN1-Quantifizierung (ICH), Neurodevelopmental Scoring, Durchführung von Verhaltenstests
- Jakob Kreye und Nina Wenke, Generierung und initiale Charakterisierung der in dieser Arbeit eingesetzten Antikörper
- Hans-Christian Kornau, Etablierung und Durchführung eines GluN1-Antikörper-spezifischen ELISA-assays
- Larissa Kraus, Durchführung und Analyse der elektrophysiologischen Ableitungen
- Melissa Long, technische Assistenz bei Verhaltenstests
- Susanne Müller, Stefan Koch und Philipp-Böhm Sturm, Durchführung, Analyse und statistische Auswertungen der Kleintier-MRTs

Mariya Chayka und Jakob Kreye bin ich besonders dankbar, da sie nicht nur immer halfen, wenn ich sie brauchte sondern mit Ihrer Art eine Leichtigkeit in den Laboralltag brachten, die mir fehlen wird.

Viele Wissenschaftler haben mich unterstützt, indem sie mir Methoden erklärten, Teilprojekte besprachen oder wertvolle Ratschläge gaben. Vielen Dank möchte ich hiermit sagen an: Hans-Christian Kornau, Stella Amrei Kunde, Ingo Przesdzing, Markus Höltje, Ana Oliveira Ferreira, Nils Rademacher, Hanna Zieger und Bettina

Schmerl. Ich danke auch den technischen Assistenten unseres Labors Doreen Brandl, Mareike Thielke und Petra Loge für die tolle Zusammenarbeit.

Auch Ulrich Dirnagl danke ich sehr, der als Erstbetreuer meiner Arbeit und Leiter der Experimentellen Neurologie mir oft bei Fragen zum Thema Übertragbarkeit von Ergebnissen weitergeholfen und mich für die Wichtigkeit des Ausschlusses systematischer Fehler vor, während und nach einer experimentellen Arbeit sensibilisiert hat.